The Journal of Experimental Biology 207, 4299-4323
Published by The Company of Biologists 2004
doi:10.1242/jeb.01262

Dragonfly flight: free-flight and tethered flow visualizations reveal a diverse array of unsteady lift-generating mechanisms, controlled primarily *via* angle of attack

Adrian L. R. Thomas*, Graham K. Taylor, Robert B. Srygley†, Robert L. Nudds‡ and Richard J. Bomphrey

Department of Zoology, Oxford University, South Parks Road, Oxford, OX1 3PS, UK

*Author for correspondence (e-mail: Adrian.thomas@zoo.ox.ac.uk)
†Present address: Smithsonian Tropical Research Institute, Unit 0948, APO AA 34002-0948 USA
‡Present address: School of Biology, Leeds University, L. C. Miall Building, Clarendon Way, Leeds, LS2 9JT, UK

Accepted 24 August 2004

Summary

Here we show, by qualitative free- and tethered-flight flow visualization, that dragonflies fly by using unsteady aerodynamic mechanisms to generate high-lift, leading-edge vortices. In normal free flight, dragonflies use counterstroking kinematics, with a leading-edge vortex (LEV) on the forewing downstroke, attached flow on the forewing upstroke, and attached flow on the hindwing throughout. Accelerating dragonflies switch to in-phase wing-beats with highly separated downstroke flows, with a single LEV attached across both the fore- and hindwings. We use smoke visualizations to distinguish between the three simplest local analytical solutions of the Navier–Stokes equations yielding flow separation resulting in a LEV. The LEV is an open U-shaped separation, continuous across the thorax, running parallel to the wing leading edge and inflecting at the tips to form wingtip vortices. Air spirals in to a free-slip critical point over the centreline as the LEV grows. Spanwise flow is not a dominant feature of the flow field – spanwise flows sometimes run from wingtip to centreline, or *vice versa* – depending on the degree of sideslip. LEV formation always coincides with rapid increases in angle of attack, and the smoke visualizations clearly show the formation of LEVs whenever a rapid increase in angle of attack occurs. There is no discrete starting vortex. Instead, a shear layer forms behind the trailing edge whenever the wing is at a non-zero angle of attack, and rolls up, under Kelvin–Helmholtz instability, into a series of transverse vortices with circulation of opposite sign to the circulation around the wing and LEV. The flow fields produced by dragonflies differ qualitatively from those published for mechanical models of dragonflies, fruitflies and hawkmoths, which preclude natural wing interactions. However, controlled parametric experiments show that, provided the Strouhal number is appropriate and the natural interaction between left and right wings can occur, even a simple plunging plate can reproduce the detailed features of the flow seen in dragonflies. In our models, and in dragonflies, it appears that stability of the LEV is achieved by a general mechanism whereby flapping kinematics are configured so that a LEV would be expected to form naturally over the wing and remain attached for the duration of the stroke. However, the actual formation and shedding of the LEV is controlled by wing angle of attack, which dragonflies can vary through both extremes, from zero up to a range that leads to immediate flow separation at any time during a wing stroke.

Supplementary material available online at
http://jeb.biologists.org/cgi/content/full/207/24/4299/DC1

Key words: dragonfly, flight, leading edge vortex, micro-air vehicles, unsteady aerodynamics, critical point theory, spanwise flow.

Introduction

Aerodynamics of dragonfly flight

Dragonflies are accomplished aerial pursuit hunters: they can hover, accelerate in almost any direction and manoeuvre precisely at high speed (Alexander, 1984, 1986; Azuma and Watanabe, 1988; May, 1991; Rüppell, 1989; Wakeling and Ellington, 1997b) to intercept other insects, with measured success rates as high as 97% (Olberg et al., 2000). The direct flight musculature of dragonflies means that stroke frequency, amplitude, phase and angle of attack can be varied independently on each of the four wings. Dragonflies put these abilities to excellent effect, using them to enlist a variety of wing kinematics in free flight (Alexander, 1984, 1986; Azuma and Watanabe, 1988; Rüppell, 1989; Wakeling and Ellington, 1997b). The wings counterstroke when cruising, but stroke in-

phase during manoeuvres and when higher accelerations are required (Alexander, 1984, 1986; Rüppell, 1989). Switching to in-phase stroking allows dragonflies to attain speeds of 10 m s^{-1}, sustainable accelerations of 2 ***g***, and instantaneous accelerations of almost 4 ***g*** (Alexander, 1984; May, 1991).

Such high performance is remarkable, but perhaps not surprising. Recent theoretical analyses (Anderson et al., 1998; Triantafyllou et al., 1993, 1991; Wang, 2000), computational analyses (Jones and Platzer, 1996; Tuncer and Platzer, 1996), and experimental analyses (Anderson et al., 1998; Huang et al., 2001) indicate that isolated flapping foils can produce high thrust coefficients together with very high efficiency if the kinematics are appropriately configured. Specifically, wingbeat frequency (*f*), stroke double amplitude (*a*) and flight speed (*U*) should combine to give a dimensionless Strouhal number ($St=fa/U$) at which wake formation is energetically efficient and a leading-edge vortex (LEV) is formed on each downstroke (Taylor et al., 2003). The LEV should remain over the foil until at least the end of the downstroke. Theoretical (Bosch, 1978; Jones and Platzer, 1996) and computational (Lan and Sun, 2001a,b; Tuncer and Platzer, 1996) analyses indicate that adding a second, trailing foil can further increase efficiency. Corresponding reductions in shaft torque and power have also been measured in flight tests using helicopters modified to allow appropriate interactions between the rotor blades (Wood et al., 1985). The direct flight musculature and four-winged morphology of dragonflies make them ideal candidates for exploiting such aerodynamic effects.

LEVs were first proposed to be a likely source of high lift forces in flying insects by Maxworthy, who demonstrated their presence experimentally on mechanical flapping models, or flappers (Maxworthy, 1979, 1981). A series of analyses using flappers with dragonfly-like wings and kinematics (Saharon and Luttges, 1987, 1988; Somps and Luttges, 1985) showed indirectly that LEVs could be important in forward flight in dragonflies, and this was confirmed directly by tethered dragonfly flow visualizations (Reavis and Luttges, 1988). Earlier analyses of tethered dragonflies 'hovering' in still air had already emphasized the role of unsteady aerodynamics (Somps and Luttges, 1985), but found stalled flows completely separated at both the leading and trailing edge, instead of a bound LEV (Kliss et al., 1989). Not surprisingly, studies using plunging flat plates in zero mean flow conditions recorded similar stalled flow structures (Kliss et al., 1989), which were found to be built up over several wingbeats.

Although the care taken in this sizeable body of work is impressive, tethered flight – especially in conditions of zero flow (Somps and Luttges, 1985) – cannot be assumed to produce flows representative of those used by free-flying insects. Previous work with tethered dragonflies refers to the use of an 'escape mode' (Reavis and Luttges, 1988), which suggests that the insects may have been trying to escape from the tether (Somps and Luttges, 1986; Yates, 1986). This interpretation is borne out by the large unbalanced side forces registered in this mode and by the extraordinarily high transient lift peaks measured for tethered dragonflies 'hovering' in still air (15–20 times body weight; Reavis and Luttges, 1988). However, since the resonant frequency of the force balance used in the latter study was only twice the 28 Hz wingbeat frequency, these extraordinarily high lift values should be treated with caution. Whilst previous tethered studies are at least indicative of the extreme capabilities of dragonfly aerodynamics (Somps and Luttges, 1986), they are almost certainly not representative of the aerodynamics of normal flight (Yates, 1986).

The accompanying studies of mechanical flappers (Saharon and Luttges, 1987, 1988, 1989) remain among the most comprehensive parametric analyses of the effect of individual wing kinematics for any insect, and are the first studies to deal with the effects of phase relationships between the wings. They also include some analysis of the effects of wing morphology on the aerodynamics – notably the effect of a corrugated wing section (Saharon and Luttges, 1987). However, one important caveat to this work is that the wings were modelled on one side of the body only, with the wing flapping from the wall of the wind tunnel. This is problematic for two reasons. Firstly, tunnel wall effects (Barlow et al., 1999) will come into play near the base of the wings. Secondly – and critically – flow visualizations with other insects (Srygley and Thomas, 2002), including dragonflies (Bomphrey et al., 2002), indicate that the LEV can extend continuously across the body from one wing to the other. This flow topology cannot be produced without a realistic interaction across the body between contralateral wings, and it is therefore qualitatively different from that produced by any of the one-sided flappers or whirling arms used to date (e.g. Birch and Dickinson, 2001; Dickinson et al., 1999; Usherwood and Ellington, 2002; Van den Berg and Ellington, 1997a,b). Even the construction of existing two-sided flappers appears to preclude such interactions because either the wings are not placed in anatomically realistic positions relative to each other, or the body is missing or anatomically unrealistic (Dickinson et al., 1999; Ellington et al., 1996; Maxworthy, 1979, 1981; Van den Berg and Ellington, 1997a,b).

Neither one-sided flappers, nor tethered flow visualizations alone, are sufficient to identify with confidence the details of the flow topology and unsteady aerodynamics associated with normal dragonfly flight. Free-flight flow visualizations with real dragonflies are required to show whether the same aerodynamics are used in normal flight as have been found in tethered flight and on one-sided flappers. This lack of reliable flow visualizations has left considerable room for speculation on the aerodynamics, with a number of workers (Azuma et al., 1985; Azuma and Watanabe, 1988; Wakeling and Ellington, 1997c) suggesting that dragonfly lift generation could be explained by conventional aerodynamics with attached flows, assuming lift coefficients in the range measured on detached dragonfly wings in steady flows (Kesel, 2000; Newman et al., 1977; Okamoto et al., 1996; Wakeling and Ellington, 1997a). Even if conventional aerodynamics *could* explain dragonfly flight this does not mean that dragonflies use conventional attached-flow aerodynamics. The qualitative nature of the flow

field generated by dragonflies has to be determined by experiment – by flow visualization.

Distinguishing the nature of flow separation in insect flight

Here we present the first flow visualizations of dragonflies flying freely in a windtunnel. We use the smoke-wire visualization technique in a very specific way: one that is common in the aerodynamic literature (e.g. for studies of jets and wakes, see Perry and Chong, 1987), but has not previously been used in studies of animal flight. Rather than describing the flow by interpreting the observed smoke patterns without using any other external information, we instead use the smoke visualizations as a tool to distinguish among the simplest set of known local analytical solutions to the Navier–Stokes equations. Rather trivially, this allows us to determine the topology of attached flows (when they are used), but much more importantly, allows us to distinguish the type of flow separation that results in the LEV (which is usually present). Formally, the local analytical solutions to the Navier–Stokes equations yielding separated flows are the hypotheses being tested in this research; sketches of the solutions we consider – the three simplest solutions yielding separated flow – are presented in Fig. 1. The Navier–Stokes equations have no known general analytical solution, but local solutions can be derived in the vicinity of critical points in the flow. The formal procedure is quite classical in aerodynamic analyses of complex wakes and jets, or of separated flows (Chong et al., 1990; Lim, 2000; Perry and Chong, 1987, 2000; Perry and Fairlie, 1974; Tobak and Peake, 1982).

The three separation patterns in Fig. 1 are the simplest local analytical solutions for flow topology that yield separated flows (Hornung and Perry, 1984), and they are also the commonest forms of separation seen in experimental studies (Hornung and Perry, 1984; Perry and Fairlie, 1974; Tobak and Peake, 1982). A pair of negative open bifurcations (where the surface streamlines converge asymptotically upon a bifurcation line and separate from the surface; Fig. 1A; Hornung and Perry, 1984; Perry and Hornung, 1984) sharing the same origin and attachment line forms the separated flow over a delta wing at moderate angles of attack (Délery, 2001). The open bifurcation is also characteristic of the footprint where a vortex touches down on a surface unsteady flow (Perry and Chong 2000). The Werlé–Legendre separation is perhaps the most well-studied separation (Délery, 2001; Hornung and Perry, 1984; Legendre, 1956; Perry and Chong, 2000; Werlé, 1962): it occurs in the unsteady region where a dust-devil touches down, near the apex of a delta wing at high angle of attack, and as the origin of the LEV on the wing top surface or fuselage of many delta-winged aircraft (Délery, 2001). Simple U-shaped separations form the LEV in dynamic stall (Hornung and Perry, 1984; Peake and Tobak, 1980; Tobak and Peake, 1982), the unsteady post-stall flow over a wing at moderate angle of attack (for example, sections 15.4.1 and 15.4.2 in Katz and Plotkin, 2001) and the horseshoe vortex flow in front of a cylinder, or adverse pressure gradient on a surface (Délery, 2001; Peake and Tobak, 1980). In the flow over a blunt-nosed ellipsoid, separation switches discontinuously (stepwise) between the three topologies in turn as the angle of attack increases (Su et al., 1990). More complex separations exist (the various 'Owl face' separation patterns for example; Hornung and Perry 1984) but these involve far more complex patterns of critical points (i.e. flow singularities) and vortex skeletons. It is possible that these complex separations occur over insect bodies (at least of the larger insects), but there are good energetic (evolutionary) reasons why insects should be adapted to use the simplest forms of separation, if possible. More complex separations involve larger sets of attached vortices,

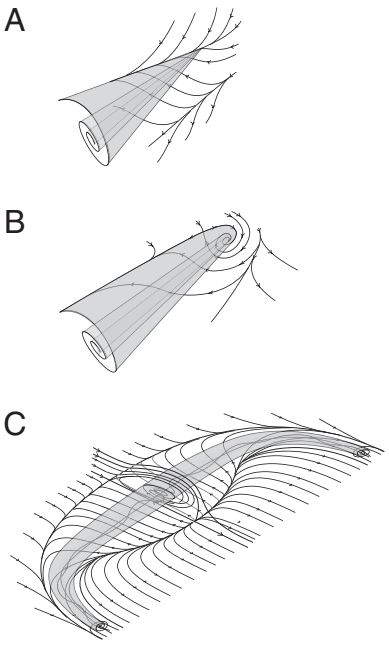

Fig. 1. Sketches of three solutions to the Navier–Stokes and continuity equations that lead to local flow separation patterns. These three types of flow separation are commonly observed in experimental situations. (A) The open negative bifurcation line consists of a negative bifurcation line from which a separatrix emerges at the front of the separation. The negative bifurcation always occurs in a pair with a positive bifurcation line. This kind of separation is often found when a vortex approaches and impacts with a surface; it is also involved in the separation over delta wings at moderate angle of attack when two symmetric negative bifurcation lines form at the leading edges and a single positive bifurcation line forms down the centreline of the delta. The negative bifurcation contains no discrete critical points, but the bifurcations – attachment and separation lines – are formed from a critical point in a cross flow. (B) The Werlé–Legendre separation has been studied since the 1960s, and occurs at the base of a dust-devil, or over a delta wing at high angles of attack. The Werlé–Legendre separation is a combination of a saddle point, from which a negative bifurcation line emerges, and a focus. The separatrix arises from the saddle point and negative bifurcation line. (C) The simple U-shaped separation occurs in dynamic stall, or in the post-stall flow over a wing. It contains a free-slip critical point (focus) above the line of symmetry, combined with a node of attachment, and the separatrix emerges from a saddle-point and the negative bifurcation (separation) lines that emerge from it at the front of the separation.

and complex multiple separations and cross flows, so they would be energetically unattractive as a fundamental topology for the LEV. We predict that insects will therefore avoid them, if they can, and hypothesize that the structure of the leading edge vortex in insect flight will involve one of the three separation topologies shown in Fig. 1. The aim of this research is to distinguish which of these topologies actually applies to the separation forming the LEV in dragonfly flight.

Flow topology is defined solely by the qualitative pattern of the streamlines, and is independent of quantitative variations in flow speed along them. Flows are topologically identical if they share the same arrangement of critical points (points where the streamline direction is undefined such as stagnation points or the centres of vortices). The exact pattern of the limiting streamlines near a surface or in the vicinity of a 3D critical point in the fluid can be solved analytically from the Navier–Stokes and continuity equations. The arrangement of their critical points constitutes the phase portrait of the flow: '*two phase portraits have the same topological structure if a mapping from one phase portrait to the other preserves the paths of the phase portrait*' (Tobak and Peake, 1982). That is, two flows are topologically identical if a deformation of the streamlines exists that can transform one pattern to the other without causing any streamline to cross itself or another. In terms of the familiar rubber sheet analogy, a surface streamline pattern, or the instantaneous streamline pattern in a 2D section of a (possibly unsteady) 3D flow, drawn on the sheet remains topologically the same, no matter how the sheet is pulled or stretched (provided there is no tearing). Qualitative flow visualizations contain the same topological information as quantitative flow visualizations; indeed, all of the fundamental work on the topology of 3D unsteady separated flows is based upon qualitative visualization techniques (for reviews, see Délery, 2001; Perry and Chong, 1987). With the many practical advantages that qualitative visualization techniques carry, it should come as no surprise that they remain an essential part of experimental aerodynamic analyses of complex separated flows (e.g. Smits and Lim, 2000).

Guided by our free-flight visualizations we are able to restrict our analysis of tethered flight sequences to those where the topology of the flow field matches what we see in free flight. Earlier studies could not reject unrealistic tethered flight visualizations because until now, there have been almost no free-flight flow visualizations with dragonflies to provide baseline data for comparison; we have obtained that fundamental data and present it here. Our free-flight visualizations are the first extensive flow visualizations of free-flying dragonflies, and of any functionally four-winged insect. The only other published flow visualizations of free-flying insects are for the butterfly *Vanessa atalanta* (Srygley and Thomas, 2002), and four images of a moth and a dragonfly (Bomphrey et al., 2002). All other previously published flow visualizations are either of tethered insects or mechanical models, and while it is assumed that these produce flows similar to those generated by free-flying insects, it remains to be demonstrated that they do. The tethered flight visualizations, by fixing the field of view, allow us to visualize flow structure with unprecedented resolution – sufficient to allow us to identify critical points in the flow around the wings, on the body, and within the LEV. The free and tethered flight flow visualizations we provide here show that whilst attached flows are typical for the hindwings in normal counterstroking flight, the forewings almost exclusively use separated flows when they generate lift (even though angle of attack can be varied to maintain attached flows on both sets of wings).

Materials and methods

Animals

We netted brown hawkers *Aeshna grandis* L., migrant hawkers *A. mixta* Latreille and ruddy darters *Sympetrum sanguineum* Muller in the Oxford University Parks. All flow visualizations were made either immediately following capture, or occasionally later that day or on the following day, in which case the dragonflies were kept cool in a refrigerated room overnight to prevent them from damaging themselves.

Mechanical flapper

A 150 mm×25 mm×0.75 mm brass plate was plunged sinusoidally by a drive box consisting of an input shaft driven by an electric motor (SD13 AC, Parvalux Electric Motors Ltd., Bournemouth, UK), with an inverter for speed control (Mitsubishi U120, Tokyo, Japan). Gears on the input shaft drive gears on the output shaft, which in turn drive the vertical movements of nylon pistons in brass cylinders *via* con-rods. The internal movements of the drive box are similar to an internal combustion engine, and because the motion is a unidirectional rotation, there is no backlash from the gears, and the sinusoidal input through pin-joints to the piston provides negligible backlash in the output drive. The plate was connected to the piston by a 3 mm diameter steel rod, passing through a small aperture in the bottom of the wind tunnel. Only the plate and supporting rod were in the flow. For the flapper experiments the plunging plate was replaced by two 75 mm×25 mm×0.75 mm brass plates hinged at the centreline and arranged so that mean angle of attack could be varied repeatably. The flapper was driven by the same drive-system, but the drive shaft was split at a Y-junction to drive each wing of the flapper and the hinge base was attached rigidly to the force balance.

Flow visualization experiments

Smoke visualizations were performed in the Oxford University Zoology Department low-noise, low-speed, low-turbulence, open-return wind tunnel, which has a contraction ratio of 32:1, working section of 0.5 m×0.5 m×1 m, and turbulence level (measured by hot-wire survey) of less than 0.3% Root Mean Square (RMS) at the 1 m s^{-1} and 2.75 m s^{-1} airspeeds used in this study. Smokelines were generated by the smoke-wire technique using model steam engine oil or Johnson's® Baby Oil on an electrically heated 0.1 mm nichrome wire. The flow velocity was 1.0 m s^{-1} for free flight

(sufficient for good smokelines) and 2.75 m s^{-1} for tethered flight (sufficient to induce sustained tethered flight). An array of DC spotlights was used to give 650 W even overhead illumination.

We first visualised free-flying hawkers and darters during take-off and manoeuvring flight in a wind tunnel. High-speed digital video recordings were obtained using one or two synchronised cameras (NAC500; 250 frames s^{-1}; 496×358 pixels). This yielded approx. 525 informative frames, from the 38 wingbeats for which the dragonflies were flying in smoke. We then tethered the hawkers to allow us to frame the image more tightly, therefore maximising frame rate and resolution (NAC500; 500 frames s^{-1}; 496×166 pixels). The hawkers were rigidly tethered to a 6-component force balance (I-666, FFA Aeronautical Research Institute of Sweden, Stockholm, Sweden SE-17290) during the high-speed flow visualizations. The tether was a 0.5 mm sheet aluminium platform cemented with cyanoacrylate adhesive to the sternum. This yielded just over 5800 informative frames of high-speed flow-visualization. High-resolution images were obtained simultaneously, using a Canon XL1 camcorder (25 frames s^{-1}; domestic compact PAL digital video, 300 000 effective pixels), and up to three Canon MV30 camcorders (25 frames s^{-1}) were used to assist reconstruction of the 3D unsteady flows from other angles. This yielded just over 2250 informative frames, giving over 8500 informative frames in total. The images we present here are unmodified, except for adjustments in overall image brightness/contrast.

Interpretation of the flow visualizations

In steady flows, for example in the laminar flow between the smoke wire and the leading edge of the insect wing, the streaklines formed by smoke are coincident with streamlines of the flow. In the unsteady flow generated by the rotating and accelerating wings (for example during pronation or supination), however, the streaklines of the smoke will deviate from the streamlines over time, because the shape of the smokelines represents not the current movement of the fluid, but the current movement plus the spatially integrated time history of recent motions. Thus care must be taken in the interpretation of individual smoke visualizations, but the problem is greatly eased by considering the movement of the flow field indicated by the smokelines in a series of images making up an animation (Perry and Chong, 2000). In this case, the instantaneous flow can be determined from the movement of the smokelines without the observer becoming overly distracted by discrete features (kinks, loops), which may represent historical, rather than actual, flow features. Animations of the high-speed video sequences referred to here are available online as Supplementary Information for this purpose.

Smoke visualizations are also problematic where vortex stretching is a major feature of the flow. Over long time scales, smoke particles may, in effect, be left behind by vortex stretching so that vortices forming important features of the flow may not be marked by smoke particles. However, problems with vortex stretching typically involve a timescale of many seconds (Kida et al., 1991), far longer than is relevant to insect flight. Dense smokelines are present in our flow visualizations within the regions of most intense vortex stretching (in the core of the leading edge and wingtip trailing vortices), which clearly demonstrates that smoke visualizations are appropriate for the analysis of the flows over insect wings.

Smoke introduced into the flow in a region where vorticity is generated, moves with the fluid. Like vorticity, the smoke pattern is Galilean invariant, so the smoke pattern does not depend on the frame of reference of the observer, making it uniquely suitable for studying insect flight where the frames of reference are extremely complex. Quantitative velocimetry data, such as instantaneous velocity vectors or streamlines, depend very much on the observer velocity and great care must be taken in selecting the frame of reference (R. J. Bomphrey, N. J. Lawson, G. K. Taylor and A. L. R. Thomas, manuscript 1 submitted; Perry and Chong, 2000). In the flow visualizations presented here, smoke is released into the flow far upstream and then passively transported by the laminar flow through the tunnel to the insect. Inevitably a particular smokeline enters the flow around the insect at the point where vorticity is being generated, passing close to, or even bifurcating at, an attachment point on the body or wings, a separation point at the leading edge, or at a free-slip critical point in the fluid above or behind the insect. The topology of the flow can be simply reconstructed by following those particular smokelines and identifying the bifurcations in them that mark the position of critical points in the flow field.

Critical point theory

A problem with previous analyses of the unsteady separated flow over the wings of flying insects is that no formal system has been used to describe the different types of flow field that insects generate. In contrast, the aerodynamic literature, since the early 1980s, has relied on the formal system provided by critical point theory to describe unsteady flow fields, especially where complex vorticity fields, 3D unsteady flows and vortex shedding processes are involved (Délery, 2001; Tobak and Peake, 1982). Critical point theory was first used by Legendre (1956) to describe steady separated flows, and it can be readily applied to skin friction lines on a body surface, to the pattern revealed by the projections of the instantaneous streamlines in any plane in a steady or unsteady 3D flow, or to the instantaneous streamlines in a steady or unsteady 3D vector field. According to Chong et al. (1989), '*Critical points and bifurcation lines are the salient features of a flow pattern. In fact, they are probably the only identifiable features of flow patterns*'. Critical point theory was first introduced to insect flight research by Srygley and Thomas (2002) to allow unambiguous description of the complex 3D separated flow topologies butterflies produce.

The direction of a streamline at any point is the instantaneous direction of motion of an infinitesimal fluid particle at that point. Legendre (1956) noted that only one streamline could pass through any non-singular point in the

vector field describing the flow, but this is not true at singular or critical points. Since the flow is modelled by a vector field, it can be described by a system of differential equations, which can lead mathematically to the existence of singular, or critical, points – points where either the direction or magnitude of the flow velocity vector is indeterminate (Poincaré, 1882). If a body is present in the flow, then there always exist at least two critical points on the surface of the body where the direction of the streamline(s) cannot be defined. This is a specific consequence of a more general topological rule due to Lighthill (1963) that we discuss shortly: the important point is that there are certain topological rules that constrain the patterns and types of critical points that can exist in real flows.

Critical points are classified into three main types: nodes, foci and saddles. Nodal points are common to an infinite number of streamlines; an example is the attachment point at the front of a wing or body. Foci are also common to an infinite number of streamlines, but differ from nodes in that none of the streamlines entering or exiting them share a common tangent line. At a focus, an infinite number of streamlines spiral around the critical point. The streamlines may spiral in to the critical point, spiral out from the critical point, or form closed paths around it (in which case the critical point is termed a centre). Centres are inherently unstable, and are transient features that tend to degenerate into foci. An example of a focus is the attachment point where a vortex touches down on a surface (like the point where a dust devil or tornado touches the ground). Saddle points are common to only two streamlines (termed separators) that pass through the critical point: the flow along one of these separators converges upon the critical point, whereas the flow along the other diverges from it. Adjacent streamlines curve between the separators, so the separators at saddle points divide the flow into distinct regions. Examples of saddle points occur wherever flows converge, and saddle points are characteristic of separated flows in general. Some authors even suggest that separated flows may be defined by the occurrence of saddle points (Délery, 2001; Lighthill, 1963; Perry and Chong, 1987; Tobak and Peake, 1982)).

Critical points define the topology of the flow, and they obey topological rules in just the same way as do the classical 3D regular solid bodies, where the number of faces plus corners must equal the number of edges plus two; for example, a cube has six faces plus eight corners and 12 edges. Similarly, Lighthill (1963) noted that the skin friction lines (limiting streamlines) on the surface of a 3D body obey the topological rule that the number of nodes plus foci must equal the number of saddles plus two, and Tobak and Peake (1982) have defined topological rules for 3D flows in general. A clear recent review of the use of critical point theory is provided by Perry and Chong (2000). Importantly, there are only a very limited number of ways of joining a set of critical points and, for simple systems of critical points, flows with the same set of critical points have the same topology. In other words, topological rules constrain the patterns of the streamlines joining the critical points (i.e. the phase portrait), so that for simple systems of critical points, knowing the nature and number of critical points can be sufficient to specify the phase portrait and streamlines of the flow.

Describing the set of critical points in the flow around an insect therefore provides a rigorous description of the topology of the flow field. The use of critical points is relatively straightforward where a complete instantaneous 3D vector field of the flow is available. Where time-dependent techniques, such as smoke visualization, are involved, the position and nature of the critical points must be inferred indirectly, but this can still be done without ambiguity. The process we use to identify critical points from the smokelines is explained in the second section of the results (see Figs 12, 14), and while we cannot identify the streamlines of the flow directly, we can identify and objectively define its topology by identifying the critical points of the flow field.

Results

Free-flight flow visualizations

Free-flying insects are, by definition, unconstrained. The vast majority of free-flight sequences with the dragonflies occur either before smoke was released, or after it had dissipated. In most cases where smoke and dragonflies were both present at the same time the dragonflies chose to fly out of the line of the smoke. Nevertheless we were able to obtain eight sequences in which the dragonfly flew through smoke and was in the field of view of at least two perpendicular cameras. In total we were able to clearly identify the flow pattern around the wings during 38 wingbeats. These represent the only existing data on the flow around the wings of free-flying dragonflies, and also represent the most comprehensive set of flow visualization data for any free-flying insect. These free-flight flow visualizations are presented as composite sequences extracted from the high-speed video recordings, to provide baseline data that can be used to check the validity of further tethered flight, mechanical model or Computational Flow Dynamics (CFD) analyses. The original video sequences are presented as supplementary material on the web.

The distribution of dragonfly free-flight flow patterns, number of wingbeats, and flight sequences in which they occur are presented in Table 1. Almost three quarters of all wingbeats (28/38) were counterstroking with a LEV on the forewing. 5/38 of wingbeats involved attached flows, usually during manoeuvres, and 4/38 involved simultaneous in-phase wingbeats – associated with accelerations. A free-slip critical point on the midline was observed during five wingbeats but those were all the wingbeats where the smoke was on the midline (dragonflies rarely crossed through the smoke). Spanwise flows were observed during ten wingbeats, and in seven of those cases the spanwise flow was from wing tip towards the wing root. Each of those cases involved sideslip either due to yaw or roll, and the inwards flow was from the leading wingtip towards the thorax. A LEV over the hindwing, stalled flow on the forewing, and zero-lift aerodynamics were each observed on two wingbeats in free flight in the windtunnel

Table 1. *Flight patterns visualized in free-flying dragonflies*

Flight pattern	Number of wingbeats where that flight pattern could be unequivocally identified	Free-flight sequences showing that flight pattern
Counterstroking		
LEV on forewing downstroke	28	*Aeshna mixta* sequence 1: (2) *A. mixta* sequence 3: (3) *Aeshna grandis* sequence 3: (7) *A. grandis* sequence 1: (3) *Sympetrum sanguineum* sequence 1: (2) *S. sanguineum* sequence 2: (11)
LEV on hindwing downstroke	2	*A. mixta* sequence 1: (1) during pitch-down manoeuvre *S. sanguineum* sequence 2: (1) during pitch-down manoeuvre
Conventional attached flows on forewing downstroke	4	*A. mixta* sequence 1: (1) forewing on pitch-down manoeuvre *A. mixta* sequence 2: (2) during roll manoeuvre at speed (forewing and hindwing) *S. sanguineum* sequence 2: (1) during pitch-down manoeuvre
Zero aerodynamic angle of attack on downstroke	2	*A. mixta* sequence 2: (2) forewing and hindwing during roll manoeuvre at speed
In-phase flapping		
LEV over both wings on downstroke	4	*A. grandis* sequence 2: (1) vertical acceleration *S. sanguineum* sequence 1: (1) take-off acceleration *S. sanguineum* sequence 2 vertical acceleration (2)
Free slip critical point visualized on centreline	5 (100% of all wingbeats visualized with smoke on the centreline)	*A. mixta* sequence 1: (1) *A. mixta* sequence 3: (2) *S. sanguineum* sequence 2: (2)
Spanwise flow in LEV?	10 (7 with spanwise flow inwards from tip to root; 3 with spanwise flow outwards)	*A. mixta* sequence 1: (2) inwards on forewing and hindwing *A. mixta* sequence 3: (1) outwards; (1) inwards *A. grandis* sequence 2: (2) outwards; (2) inwards during roll/sideslip *S. sanguineum* sequence 2: (2) inwards during yaw/sideslip
Stalled (flat-plate) flow	2	*A. mixta* sequence 3: (1) initiation of roll on forewing upstroke *S. sanguineum* sequence 2: (1) on forewing at end of pitch-down manoeuvre

LEV, leading edge vortex.

S. sanguineum sequence 2 is video S1 in supplementary material; *A. mixta* sequence 1 is the first section of video S2 in supplementary material; *A. mixta* sequence 3 is the second section of video S2 in supplementary material; the other sequences do not appear in supplementary material.

during control manoeuvres. However, our dragonflies flew gently in the windtunnel – never even approaching their maximum aerodynamic performance; speeds of $10\,m\,s^{-1}$, sustainable accelerations of $2\,\boldsymbol{g}$, and instantaneous accelerations of almost $4\,\boldsymbol{g}$ (Alexander, 1984; May, 1991).

Unstructured wake in free-flying dragonflies

The interaction between the wings and the shed LEV leads to an unstructured wake devoid of the vortex loops that have been assumed to connect vortices shed at the top and bottom of each stroke in most theoretical models of insect flight.

The wake of free-flying dragonflies is illustrated in Fig. 2, where smoke is on the centreline of the animal, and Fig. 3, where the smoke plane is close to the wingtip (also see video S1 in supplementary material). In both cases the wake is characterised by a lack of any coherent structure. The wingtip vortices are clear in Fig. 3, but can be seen in the wake visualizations for less than 1/50th of a second. Whether they dissipate on this timescale or not is uncertain. Comparing Figs 2 and 3, it is clear that although the wingtip vortices form discrete wake elements in Fig. 3, these have no counterpart – there is no starting vortex – at the centreline in Fig. 2. Therefore the shape of the wake shed from each wingbeat is complex, lacking a starting vortex, but with the curved paths of the wingtip trailing vortices following the curved path taken by the wingtips, and then being closed off by the vortex shed

into the wake at the end of the downstroke. This flow pattern is strikingly reminiscent of the flow generated by a jet in a cross-stream (Smits and Lim, 2000).

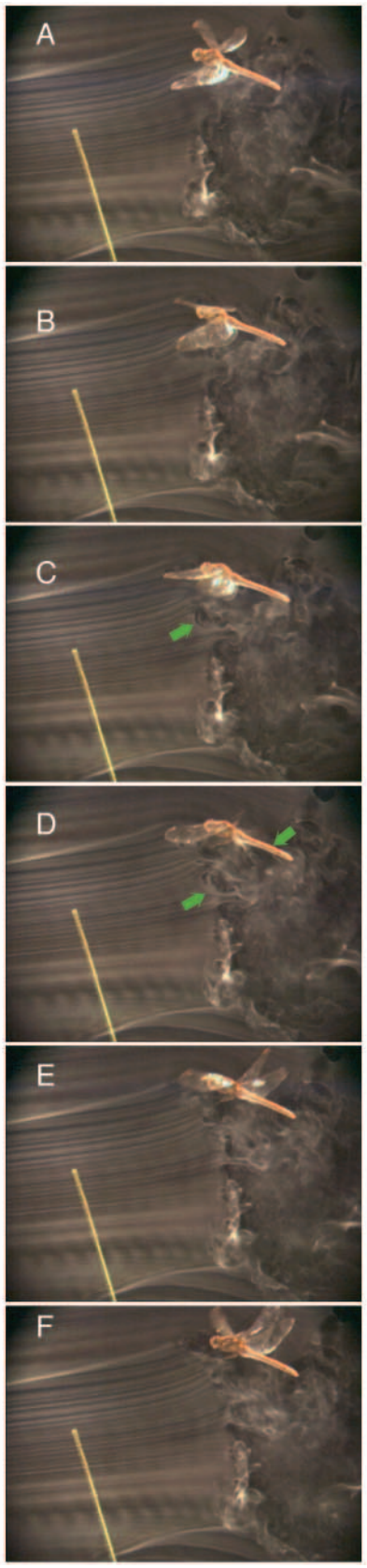

Use, formation and structure of the leading edge vortex in free flight

Counterstroking is the normal flight mode used by dragonflies. The LEV in counterstroking is visualised in Fig. 4, where the dragonfly has just taken off and is flying sideways, holding station next to its perch, against the 1 m s^{-1} flow through the windtunnel. The LEV in counterstroking flight is bounded by a separation near the leading edge, with the separatrix touching down at a stagnation point on the top surface of the forewing near the trailing edge. Thus the separation containing the LEV is similar in size to the wing chord. In the image-sequence of Fig. 4 the intersection of the smoke plane with the wing moves from the wingtip towards the centreline, and the LEV is similar in size and consistent in structure at each station along the length of the wing. The structure of the LEV at the midline, over the wing hinge and thorax is clear in Figs 8, 9, the LEV is continuous across the wing span, and is unchanged as it crosses the wing hinge onto the thorax. More detail of the structure at the centre of the LEV above the thorax is provided by the tethered flight flow visualizations below.

Although the flow is generally attached in counterstroking flight, this may not be the case during manouvres. Rapid increases in angle of attack can cause the formation of a LEV at any stage of the wingbeat on either fore or hindwings. Fig. 5 shows a sequence in which the dragonfly performs a pitch-down manouver – a manouver requiring large nose-down pitching moments. The dragonfly performs this manouver by rapidly increasing the angle of attack of the hindwings, during the second half of the downstroke, as can be seen from the increase in the projected height of the wing chord. As the hindwing angle of attack increases the initially attached flow over the hindwings separates to form a LEV that grows as the wings rotate, persisting beyond the end of the downstroke. In contrast, Fig. 6 shows a sequence where the dragonfly is initiating a roll to the right – a manouver requiring reduced forces from the wings on the right side of the body. Smoke streams over the right forewing show little displacement as the wing cuts through them on the upstroke – symptomatic of an unloaded upstroke – and then show no evidence of any flow separation on the subsequent downstroke. The flow over the forewing matches what would be expected for conventional

Fig. 2. Free-flight flow visualization of the wake of the dragonfly *Sympetrum sanguineum* in counterstroking flight. (A–F) Composite figure of sequential images extracted from a 250 Hz high speed video recording (video S1 in supplementary material). The dragonfly is moving from left to right through the smoke plane, which is approximately at the near wing hinge in (A). Wake structure is incoherent. There is no sign of a starting vortex, but some sort of vortex structure (stopping vortex? Wingtip vortex in oblique view?) is apparent in (C–E) (green arrows) and a wake element of sorts can be seen between the green arrows in (D). This wake element rapidly loses its identity after it is shed, being hard to detect after two frames (1/125th of a second). The visualised wake is not consistent with a series of discrete vortex elements such as, for example, vortex rings.

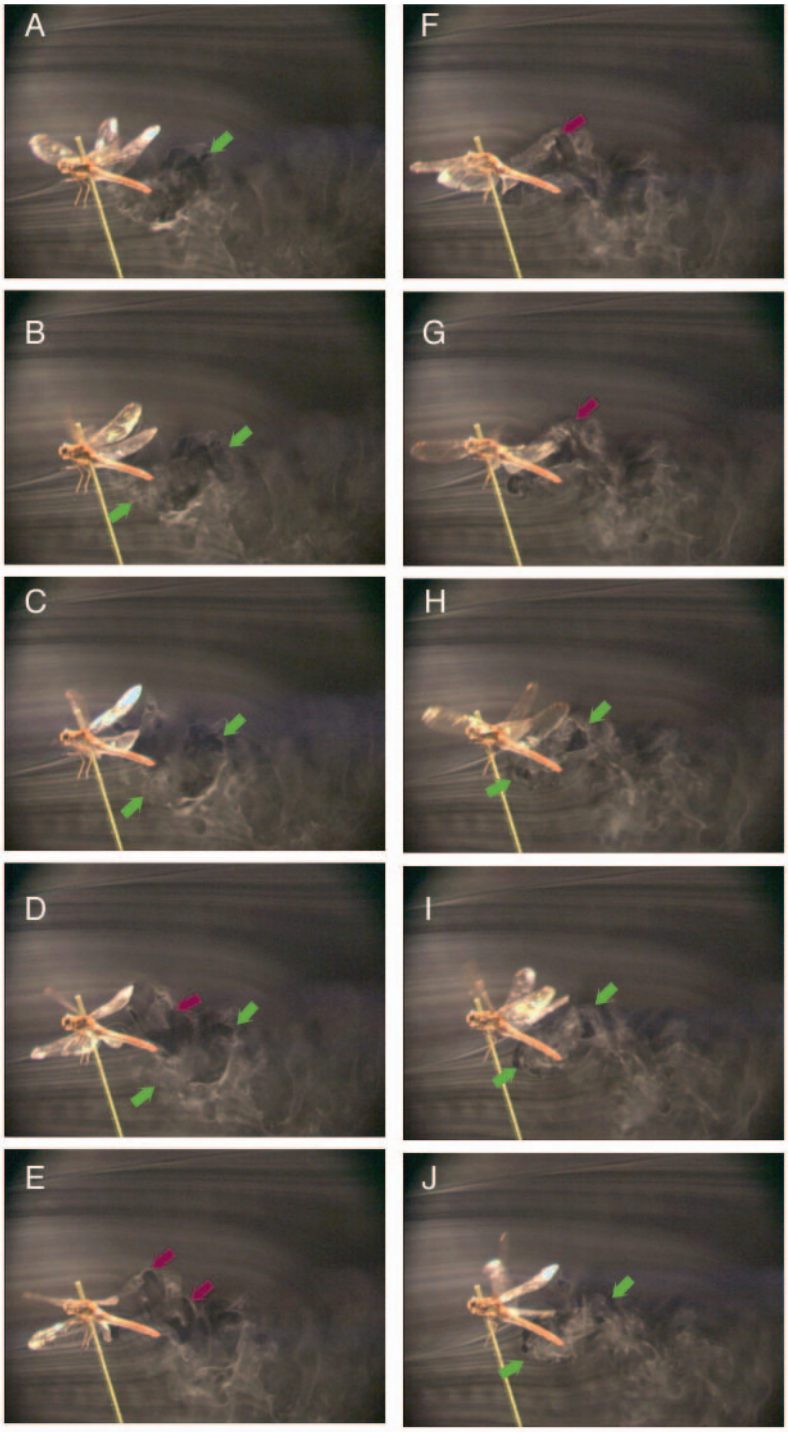

Fig. 3. Free-flight flow visualization of the wake of the dragonfly *Sympetrum sanguineum* in counterstroking flight with the smoke-plane close to the right (far) wingtip. (A–J) Consecutive images from a 250 Hz high-speed video recording. In contrast to the centreline flow shown in Fig. 2, here the wingtip vortices are clear (purple arrows), and form wake elements (green arrows) that persist for several frames. However even here at the wingtips, where the wake structure is at its most coherent, the wake elements lose their identity after five frames (A–E, 1/50th of a second). The difference between the apparent structure of the wake elements between the tip region and the centreline region suggests that wake elements have a complex structure, consistent with the lack of any defined starting vortex.

attached flow aerodynamics during the downstroke in Fig. 6. Figs 5 and 6 provide typical examples of the same dragonfly operating with, or without, a LEV in the ways that would be expected if they were using the increased forces associated with the LEV to control and initiate manouvers.

Free-flying dragonflies switch from counterstroking to in-phase stroking to generate elevated forces (Alexander, 1984; Rüppell, 1989). The qualitative aerodynamic consequences of in-phase stroking are shown in video S1 in supplementary information and in Fig. 7. A LEV forms on the forewing during pronation. The forewing then undergoes a curtailed downstroke, at the same time as the hindwing undergoes an extended downstroke with particularly extreme supination, such that the forewing catches up with the hindwing as it begins its upstroke. The LEV remains attached to the forewing throughout supination, but the point of reattachment shifts back off the forewing and onto the hindwing. The single LEV so formed remains over both pairs of wings throughout the first half of their combined upstroke. This results in an even higher degree of flow separation, with a single LEV extending over the combined chord of both wings, as if over a single continuous surface: the flow separates at or near the leading edge of the forewing and reattaches on the upper surface of the hindwing. As in the counterstroking flight mode, the qualitative results are clear: the LEV is continuous across the thorax, with a free-slip focus over the midline. The flow topology becomes complex and variable towards the wingtips: the LEV inflects to form a single tip vortex when the wings are held close together, but the structure of the tip vortex is complex, and as wing spacing increases it separates into two distinct tip vortices. Although their wings are completely unlinked, in-phase stroking in dragonflies resembles in-phase stroking in functionally two-winged insects, with qualitatively the same flow topology as visualised on free-flying butterflies, where the LEV is very much smaller relative to the wing chord (Srygley and Thomas, 2002).

Unloaded upstrokes in free-flying dragonflies

The smokelines were usually scarcely deflected by the forewing during the upstroke (e.g. Fig. 6), indicating that it was only weakly loaded if at all. Negative loading (force directed towards the morphological ventral surface of the wings indicated by a dorsally directed deflection of the smokestreams) was never observed in free flight, and in tethered flight was only seen for brief periods at the end of the forewing upstroke. On the rare occasions when negative loading was observed it

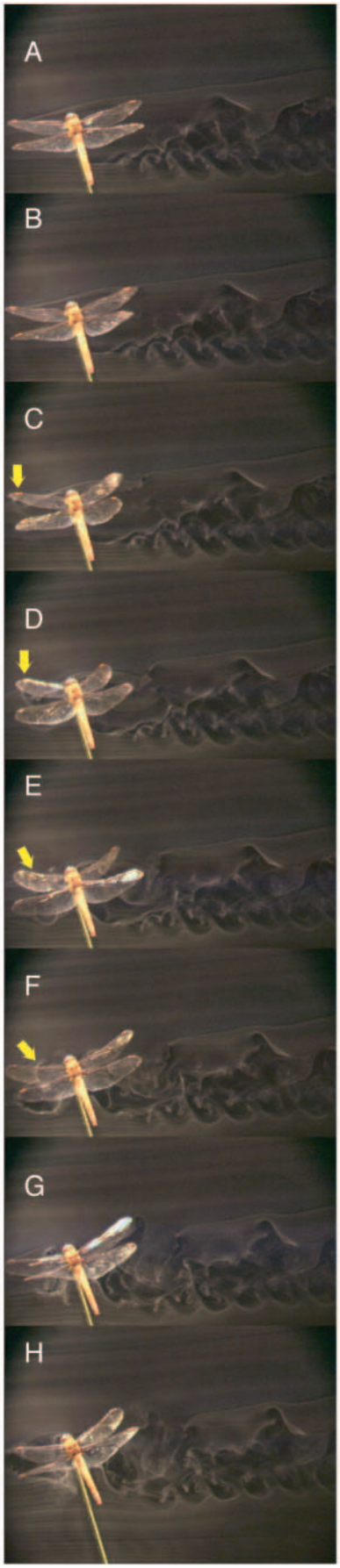

caused torsion and marked ventral spanwise bending of the wings, which could have important implications for the structural mechanics and aerofoil design of dragonfly wings (Kesel, 2000; Sunada et al., 1998; Wootton et al., 1998).

Attached flows on loaded and unloaded downstrokes in free-flying dragonflies

In some decelerating or sinking flight manoeuvres requiring low aerodynamic force coefficients, the flow over both pairs of wings remains attached on the downstroke as well (Fig. 6). Attached flows cannot provide the very high lift coefficients that LEVs can, but since they are also expected to produce much less drag, and higher lift-to-drag ratios, they might be used for efficient cruising flight (a behaviour we observed in only two free flight sequences in the constricted space of the windtunnel). Attached flows are only achieved at very low angles of attack, which reinforces our conclusion that angle of attack is the most important kinematic variable governing aerodynamic mechanism in dragonflies. In some attached flow sequences, the wings slice the smokelines like a knife (Fig. 6, the same flow pattern is seen in more detail in tethered flight in Fig. 11), indicating that dragonflies can accurately select zero angle of attack for zero lift production. This mechanism is adopted during decelerating manoeuvres involving loss of altitude. The same mechanism was used in pitch or roll manoeuvres as a means of generating large force imbalances between ipsilateral or contralateral wing pairs, without the need to take a negative load.

On the insignificance of spanwise flow in free-flying dragonflies

Previous work has implicated tipward spanwise flow through the vortex core in stabilising the LEV (Willmott et al., 1997). Spanwise flow is visualised in some of our images by smokelines drawn out of plane. For example, Figs 8 and 9 show dragonflies flying with a degree of sideslip, with the LEV visualised over the leading wing in Fig. 8 and over the trailing wing in Fig. 9. The plane of the smoke streams is distorted in opposite directions in the two images – bulging towards the centreline in Fig. 8 and towards the wingtip in Fig. 9. The bulge in the smoke plane indicates spanwise flow in opposite directions in the two images. The LEV is stable throughout such manoeuvres (Figs 8 and 9), so in a qualitative sense

Fig. 4. Free-flight smoke visualization of the flow around the wings of *Sympetrum sanguineum*. There is a leading edge vortex (yellow arrows) on the fore-wing counterstroking flight. (A–H) Consecutive images from a 250 Hz high-speed video recording. Perpendicular views from the b and c cameras show that the dragonfly has taken off and cleared the perch and is holding station, flying sideways in (A) as the forewing completes the upstroke. The downstroke begins in (B), and the LEV is already present when the wing cuts the smoke in (C). The structure of the LEV is consistent as the intersection of the smoke and the wing moves towards the midline (D,E), and the internal flows within the LEV are clear in (F). The LEV is shed at the start of the upstroke in (G). There is no evidence of spanwise flow.

spanwise flow is not necessary to stabilise the LEV. This clear qualitative result is consistent with recent experiments showing that blocking any spanwise flow on a flapping wing does not destabilise the LEV (Birch and Dickinson, 2001). More recent experimental analyses suggest that spanwise flows are only present, even on mechanical flappers, at the higher Reynolds numbers relevant for *Manduca sexta* (Birch et al., 2004), and which are in the range used by our dragonflies. However, recent theoretical analyses point out that spanwise flows may never be necessary for LEV stabilisation, given the kinematics and aerodynamic timescales used by real insects (Wang et al., 2004).

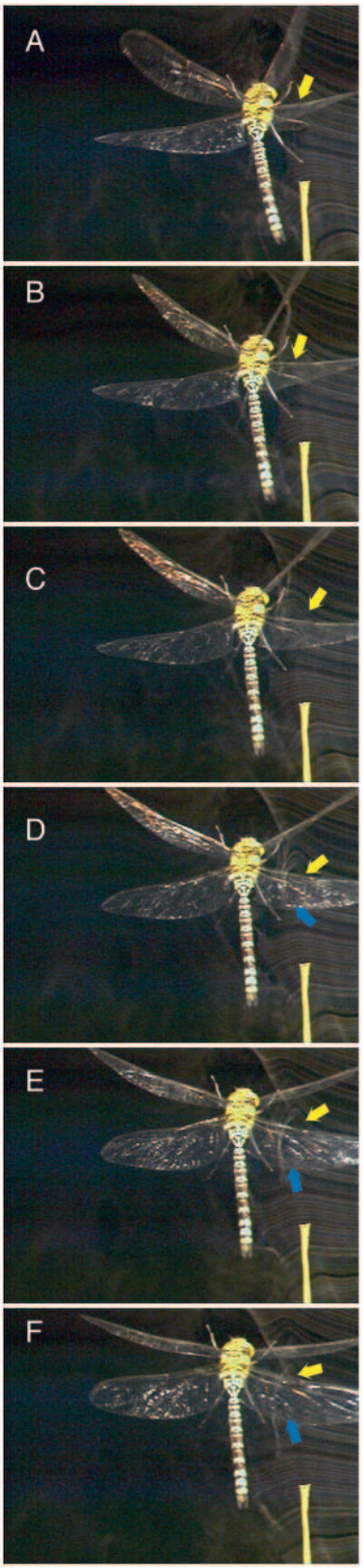

Fig. 5. Free-flight smoke visualization of the flow around the wings of *Aeshna mixta* executing a pitch-down manouver. (A–F) Consecutive images from a 250 Hz high-speed video recording. Rotation of the hindwing at the end of the downstroke causes a rapid increase in angle of attack, and initially attached flow over the hindwing separates to form a large leading edge vortex. In (A) the flow is still attached over the hindwing (yellow arrow), but in (B), as the wing rotates, increasing angle of attack, the flow separates (yellow arrow) forming a small separation bubble. This increases in size in (C), and in (D) the stagnation point where the separatrix touches down on the top surface of the hindwing is visualised (blue arrow). The LEV continues to grow as angle of attack increases in (E), and still has not been shed in (F), at the beginning of the upstroke. There is no evidence of any spanwise flow.

Variations in the aerodynamics of free-flying dragonflies

Further variations in the aerodynamics are apparent during free-flight manoeuvres, and confirm that changing angle of attack is important in LEV formation. Fig. 5 (Video S2 in supplementary material) includes a LEV formed over the hindwing by supination during a pitching manoeuvre in free flight (a LEV was also frequently formed on the hindwing during tethered flight performances by *A. mixta*, with identical flow topology to that on the forewing downstroke). We also observed (on one wingbeat) a dragonfly with stalled flow on the forewing during a climb (penultimate frame of video S2). Stalled flows are a common feature of the tethered flight performances, where they may be artefacts of tethering.

Tethered flight flow visualizations

Tethered flight is not free flight, and tethered flight flow visualizations should be treated with caution, because tethered insects can produce flow patterns that are never seen in free flight. However, by constraining the insects to one position we are able to zoom in and focus on the smoke plane, increasing the resolution of the flow-visualization images. Uniquely, here, we have the free-flight data to guide us in identifying flow-patterns in tethered flight that correspond to flow patterns observed in free flight, and more importantly (and in contrast to all previous work on tethered flying insects) we are able conservatively to treat with caution those visualization images showing flow patterns that do not match those seen in free flight.

Baseline data – flow over static dragonflies, or dragonflies flapping but generating no lift

To highlight the components of flow that are due to active

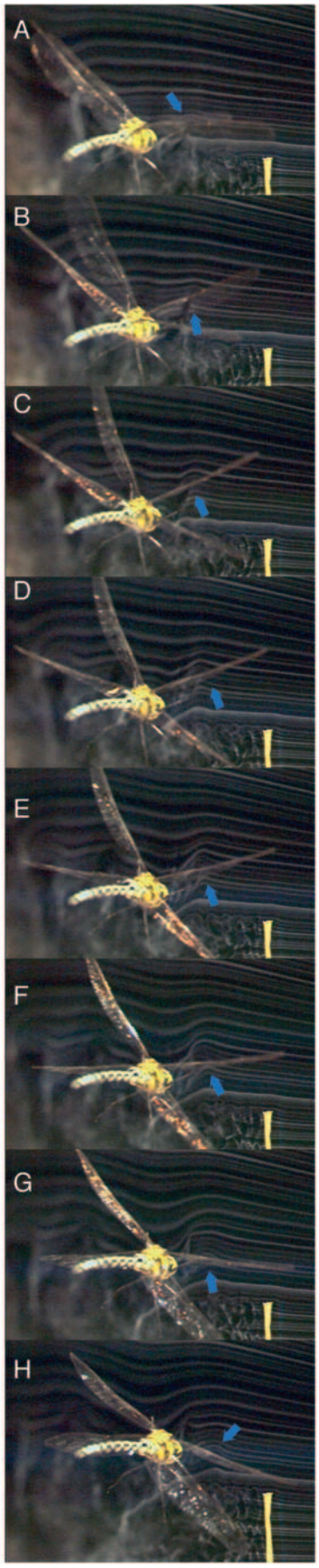

flapping and lift generation by the dragonflies, Fig. 10 shows the flow around tethered dragonflies that are static and in Fig. 11 the dragonflies are flapping but feathering their wings to zero aerodynamic angle of attack (as told by the shearing flows with negligible smokeline deflection).

The flow around stationary insects (Fig. 10) consists of a bluff-body wake behind the body of the insect, and a set of Karman streets behind the wings. The flow over the head and forward thorax is attached, but separates near the hindwing root to form an unstructured wake, with no obvious periodicity or concentrations of vorticity. As expected with a bluff-body wake, the disturbance due to the thorax is limited to the region downstream, and does not extend above the body to any appreciable degree. The wings shed vortices periodically in a Karman street, indicating that they maintain some small angle of attack even when the dragonfly is quiescent.

In contrast, in both free flight (e.g. Fig. 6) and in tethered flight the dragonflies would occasionally choose to flap with their wings held at an angle of attack so close to zero that no Karman vortex street was generated (Fig. 11). The absence of a Karman street behind the wings shows that the angle of attack is very close to zero – it is a well-known result for sharp-edged flat plates that flow separates at less than 2° positive or negative angle of attack, and that once the flow separates the flow field becomes time dependent, with wake oscillations generated by the unstable shear layer behind the trailing edge forming a Karman street in the wake (see, for example, Werlé, 1974; Van Dyke, 1988, plates 35 and 36; Katz and Plotkin, 2001, p. 508). Tethered dragonflies and dragonflies in free flight regularly achieved this flight condition during active flapping, but not during inactive flight (as can be seen in Fig. 10), suggesting that the wing is not feathering to the flow passively, and therefore suggesting that active control is involved. We were unable to replicate this flow pattern with isolated dragonfly wings even with 0.1° precision control of angle of attack at the base. This is presumably because the wings acquire a twist once they are removed from the insect, and further supports the suggestion that precise control of angle of attack is necessary to generate this flow.

The shape of the displacement of the smoke streams where they are cut by the wings in Fig. 11 reflects the nature of the boundary layer. Distortions of the smoke streams (and the

Fig. 6. Free-flight smoke visualization of the flow around the wings of *Aeshna mixta* executing a roll to the right in counterstroking flight. The flow field matches that which would be expected with conventional attached-flow aerodynamics. (A–H) Consecutive images from a 250 Hz high speed video recording. In (A–C) the wing is completing the upstroke and can be seen (blue arrows) to have sliced through the smoke streams like a knife – causing no vertical displacement. This suggests that the sections of the wing intercepting the smoke plane are generating little or no lift. The wing rotates in (C) and (D) at the beginning of the downstroke, and the flow exhibits a downwards deflection indicating lift-generation, but the smoke streams pass smoothly over the wing with no evidence of flow separation. The flow remains attached until the end of the downstroke in (H), as the dragonfly executes a roll to the right.

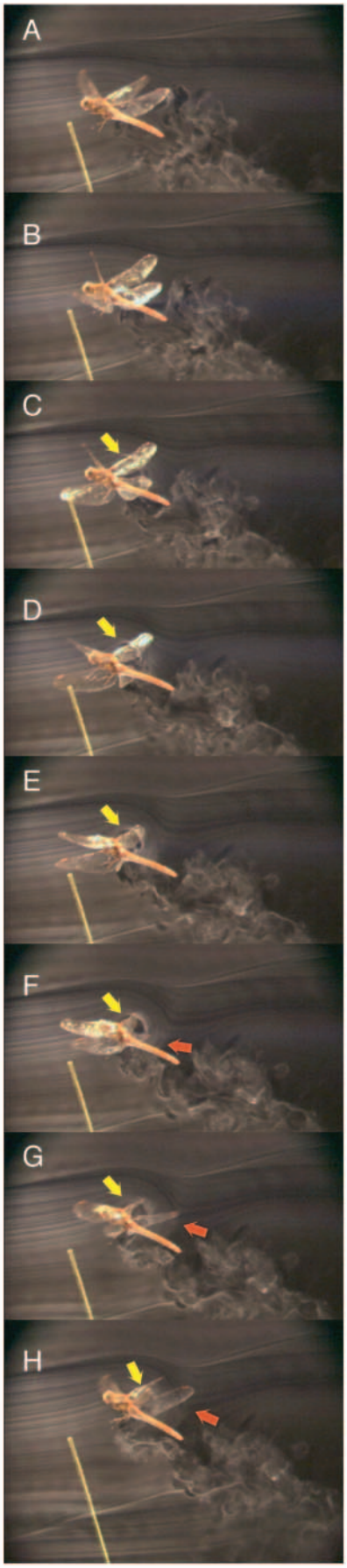

complex frame of reference) make detailed interpretation difficult. However, the wake is roughly 1 mm thick immediately behind the trailing edges of both the fore- and hindwings in Fig. 11A and behind the forewing in Fig. 11B. The boundary layer is expected to remain laminar over the whole chord at the Reynolds numbers at which the wing operates (Re≈4300). For comparison the Blasius solution for the boundary layer thickness ∂_{99} of a flat plate at a point a distance $\times$ downstream of the leading edge is $\partial_{99}=5x/Re^{1/2}$ (Katz and Plotkin, 2001, p. 461), which takes a value of 0.75mm at x=10 mm (i.e. immediately behind the trailing edge), assuming a local wing velocity of 5 m s^{-1}; this suggests that the boundary layer over the dragonflies wing is not dissimilar to the laminar boundary layer on a thin flat plate, despite the corrugations of the profile.

Identifying critical points in the dragonfly flow visualizations

Fig. 12 presents a collection of tethered flight flow visualizations, with the dragonflies flapping actively, where critical points in the flow are particularly clearly marked. In these visualizations, by chance, individual smokelines hit precisely at a critical point, or on a line of critical points such as an attachment line. Smoke particles can only be passively transported with the fluid, so that bifurcation of the smokeline at a discrete point implies a splitting of the streamline at this point (historical if not instantaneous). At the point where the smokeline bifurcates, the direction and velocity of the flow is obviously undefined, which is diagnostic of a critical point (because a critical point is the only place where streamlines cross, where velocity and direction are undefined – it is a singularity in the flow field): smokeline bifurcation unambiguously identifies the position and nature of a critical point.

The simplest critical points to understand are at attachment points and attachment lines. These are indicated in Fig. 12 by the blue arrows. Attachment points on the head are clearly marked by smokeline bifurcations in Fig. 12E,G. Attachment

Fig. 7. Free-flight smoke visualization of the flow around the wings of *Sympetrum sanguineum* accelerating vertically with the wings stroking in-phase. A leading edge vortex (yellow arrows) forms and grows to extend over both sets of wings. (A–H) Consecutive images from a 250 Hz high-speed video recording. The dragonfly is moving from left to right through the smoke plane and the smoke is approximately 1/4 wing-length in (A) and coincident with the wing hinge in (H). (A) The end of the upstroke. (B) During the forewing rotation prior to the downstroke, there is some evidence of the start of LEV formation. In (C) the LEV is already clearly formed (yellow arrow). In (D–F) the LEV rapidly grows, the smoke streams within the LEV are thinned by the increased velocities in that region making it darker, and the stagnation point where the separatrix touches down moves aft from the forewing onto the hindwing. In (F–H), as the downstroke ends and the wing rotates, the LEV is shed into the wake. There is a saddle-point (red arrows) in the wake where smoke-streams bifurcate in the shear layer between the current LEV and the wake-vortex representing the LEV shed from the previous wake. There is no evidence of any spanwise flow.

lines on the undersurface of the wing are unambiguously marked by smoke bifurcations in Fig. 12A–C, and on the top surface of the hindwing in Fig. 12B.

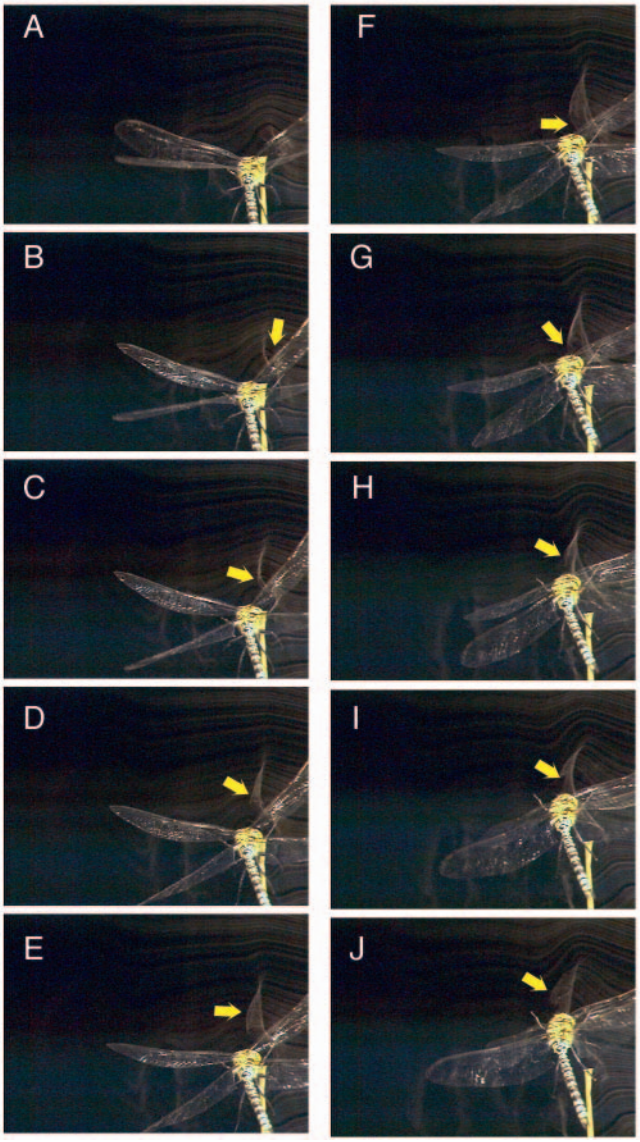

Fig. 8. Free-flight smoke visualization of *Aeshna mixta* in counterstroking flight flying with increasing left roll and yaw and consequent side-slip. There is a leading edge vortex near the midline (above the wing hinge), which exhibits spanwise flow running from the wingtip towards the centreline. (A–J) Consecutive images from a 250 Hz high-speed video recording. (A) shows the end of the upstroke, the dragonfly is aligned with the flow, with little roll or yaw, and the smoke streams form a vertical plane. In (B) the dragonfly begins the downstroke and a LEV is formed (yellow arrow), the dragonfly has also begun to roll and yaw to the left. In (C) the LEV grows, and the vertical plane of the smoke streams is distorted so that the centre of the LEV bulges towards the midline at the yellow arrow indicating a spanwise flow towards the midline. In (E–H) as the yaw increases and the LEV grows during the downstroke the bulge in the smokestreams caused by spanwise flow towards the midline also increases. The LEV is still present at the end of the downstroke in (I) and at the beginning of the upstroke in (J).

Two forms of free-slip critical point occur. The free-slip critical point (focus) above the thorax is indicated by a yellow arrow throughout Fig. 12 whenever it is visualized, and although the structure of this critical point is complex it is unambiguously marked by smoke bifurcation in the diagonal close-up views of Fig. 12H,I, where the smokelines match remarkably well the solution trajectories (streamlines) of the open U-shaped separation predicted from local analytical solution of the Navier–Stokes equations (Fig. 1). There is also a free-slip critical point in the form of a saddle indicated by the red arrow and unambiguously marked by smoke bifurcations in Fig. 12D–F,I. This saddle point marks a pressure maximum in the shear flow between the LEV over the wing, and the shed vortex in the wake. Its presence is diagnostic of the fact that the wake is one-sided – consisting of a series of vortices each of the same sign (starting vortices would have opposite sign; they are not found in the flow generated by dragonflies).

The leading edge vortex in dragonflies is continuous across the midline with a free-slip critical point above the thorax

Fig. 13 shows a series of smoke visualizations stepping across the thorax of *Aeshna grandis* in tethered flight. The flow pattern, shape, size and structure of the LEV is consistent at all positions across the thorax, and from wingbeat to wingbeat. A LEV is present in all images, and the shape and size of the LEV is consistent across the thorax and out onto the wing. The shape and size of the leading edge vortex is strikingly consistent, even though the wing chord and velocity changes dramatically as we step along the wing, across the narrow wing base onto the thorax. This is a remarkable result, suggesting that while the wings form the LEV the local details of their shape, size and motion are not amongst the principal parameters controlling LEV morphology.

Counterstroking aerodynamics – the leading edge vortex in normal flight

The same smoke pattern (Fig. 14) typifies counterstroking in all three species of dragonfly, appearing in c. 75% of wingbeats in free flight. This seems to be the normal mode of flight in dragonflies. The forewing downstroke is characterised by almost-circular smokelines immediately above the wing, suggesting the presence of a large LEV over the forewings (Fig. 4). Conventional attached flows characterise the forewing upstroke and the entire hindwing stroke.

A stagnation point is present on the undersurface of the wing near to the leading edge (blue arrows in Fig. 14, particularly well marked in Fig. 14D), and this is the simplest critical point to identify: smokelines hitting ahead of this stagnation point pass forwards to the leading edge, whereas smokelines hitting aft of the stagnation point run back to the trailing edge. Smokelines that hit exactly at the stagnation point bifurcate (Fig. 14D). In images where smoke does not impact the underside of the wing close enough to the stagnation line to bifurcate, its existence is implied by the smokelines impacting aft of the stagnation line, which run straight to the trailing edge

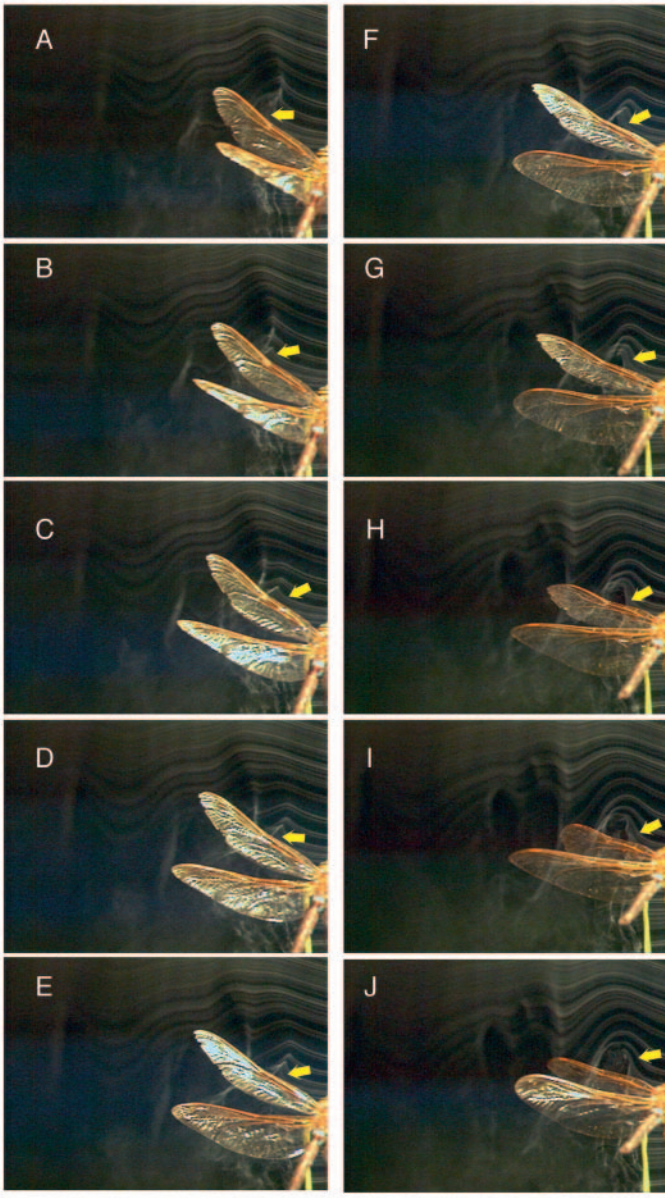

Fig. 9. Free-flight smoke visualization of the flow over the wings of *Aeshna grandis* flapping in-phase in level flight, but with a slight yaw to the left. The process of leading edge vortex formation is visualised, and the LEV has spanwise flow from the centreline towards the wingtip. (A–J) Consecutive images from a 250 Hz high-speed video recording. The leading edge vortex forms over the forewing in image sequence (A–C) at the start of the downstroke. Although the fore-wing moves upwards between images B and C, the wing rotates in a nose-down sense about an axis of rotation close to the mid-chord. This must cause a local increase in angle of attack at the leading edge, and the separation bubble that develops into the LEV forms during this phase of motion (yellow arrows). The smoke streams at the centre of the LEV are distorted in (D), bulging out towards the wingtip, which shows that there is a spanwise flow from centreline towards the wingtip – the opposite direction to that seen in Fig. 6. The bulge in the leading edge vortex is still present in (E), but decreases in (F) and is no longer apparent in (G–J), indicating that there is no longer a spanwise flow within the leading edge vortex as the wings approach the end of the downstroke and the LEV expands to cover both fore- and hindwings. The shear layer (secondary vortices?) within the leading edge vortex is apparent in (H–J), and the LEV has lifted off from the leading edge of the forewing in (J) as indicated by the presence of a smoke bifurcation at the point of the yellow arrow.

(Fig. 14B), and by smokelines impacting just ahead of it, which run forwards around the wing leading edge – the divergence of these smokelines implies that somewhere between them a streamline would hit the surface and stop at a critical point, all adjacent streamlines diverging towards either the leading or trailing edges of the wing. Each smokeline bifurcation therefore marks one of the 2D critical points that in 3D form a stagnation line (line of attachment) running parallel to the wing leading edge and emanating from a node of attachment (N1) on the head. That node of attachment is visualised directly whenever a smokeline hits between the insect's eyes and splits above and below the head (Fig. 14E). One smokeline hits the node of attachment between the insect's eyes and splits. Streamlines adjacent to that one radiate out from the node of attachment as the flow passes around the insect's head and on towards its thorax.

Smokeline bifurcation also occurs just ahead of the forewing trailing edge on the wing's upper surface, whenever a smokeline curves down to impact upon the top surface of the wing (Fig. 14B,D). Each bifurcation marks one of the 2D critical points that in 3D form a line of attachment emanating from a second node of attachment (N2). The smokeline bifurcation indicates reverse flow ahead of the line of attachment, because one of the arms of the bifurcation runs forwards from this point. Inevitably, this reverse flow running from the line of attachment near the trailing edge forwards towards the leading edge must converge with the flow running backwards from the leading edge towards the trailing edge. Separation occurs where these converging flows meet. Flows converging along the line of bilateral symmetry of the thorax will run parallel to this centreline, so symmetry requires a saddle point (S) to exist between the wing bases, on the centreline of the animal (in asymmetric flight, a saddle would still exist but would be of non-canonical form and might be displaced from the midline).

The rules of critical point theory – of topology – require that there be two more nodes than saddles on a surface in a flow (Lighthill, 1963), so a node of detachment (N3) must exist at the back of the thorax or on the abdomen, continuous with the rearward separation line (line of detachment) at the wing trailing edge. By the time the smoke has reached the abdomen, it is too disrupted by flow separation and the unsteady flow fields it has passed through to reveal this node of detachment directly. However, the existence of the rearward separation line along the trailing edge of the wing is indicated by the presence of a shear layer, or vortex sheet, smoothly leaving the trailing edge (Fig. 14D). This shear layer is visualized by smokelines flowing back along the undersurface of the wing from the forward stagnation line. Although the smokelines show that the flow departs smoothly from the trailing edge, the resulting

vortex sheet quickly rolls up into a series of small transverse vortices under Kelvin–Helmholtz instability (Saffman and Baker, 1979).

Whenever a smokeline passes close enough to the separation line on the upper surface of the wing, it lifts off the wing surface and spirals in on itself (Fig. 14C). Although smokelines can become curved in the absence of a vortical flow, spiralling smokelines can only be formed in the presence of a vortex. Spiralling of the smokelines close to the separation line therefore indicates that the separation surface becomes entrained in a vortex structure. Because the flow separates at or near the leading edge, this vortex is classified as a leading-edge vortex (LEV), and because the flow reattaches on the wing behind the vortex, the vortex is a bound LEV.

Smokelines over the thorax adopt the same pattern as over the wings (Figs 12D-I, 13, 14E, 16), so symmetry implies that there is a free-slip focus (F) above and between the forewings. Although the terminology for 2D critical points and 3D critical points on a surface is clear and well defined, 3D free-slip critical points are altogether more complex. The structure above the centreline is a free-slip critical point (Tobak and Peake, 1982) specifically, a free-slip 3D focus (Perry and Chong, 1987; Tobak and Peake, 1982). In the case where there is a free-slip critical point on the line of symmetry of a simple U-shaped separation, the separatrix from the node of separation on the head or thorax is open. A narrow band of streamlines between the separatrix and the streamline that impacts the node of attachment spirals in to the free-slip critical point under the influence of vortex stretching as the arms of the U-shaped separation extend into the wake. This complex 3D flow can indeed be seen in Figs 12H and I and 14E. The LEV extends out from this free-slip 3D focus to the tips of the wings, where it is continuous with the wing-tip vortices (Fig. 14A). The critical points identified above and in Fig. 14 are the minimum number both consistent with the topological rules of fluid flow

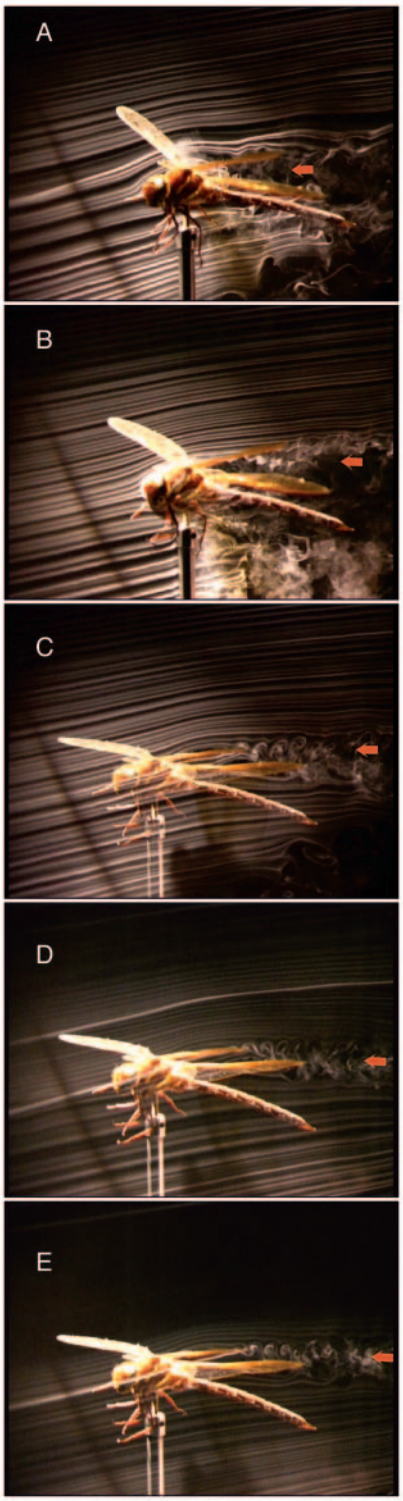

Fig. 10. (A–E) Smoke visualization of static tethered dragonflies. The dragonflies are still, and the images represent baseline data showing what the flow around the dragonflies looks like when they are not flapping. The successive images step from the right (far) wing hinge across the thorax and out along the near wing. In (A) the smoke plane is aligned with the far wing hinge, and smoke flows smoothly past the 5 mm diameter mount below the insect, becoming incorporated in the Karman street (red arrow) behind the mount far downstream. The flow over the thorax is attached back to the hinge of the hindwings, and then separates to form an unstructured wake behind the body. In (B) the smokeplane is on the midline, and the smoke hits the dragonfly between the eyes. Below the dragonfly the smoke is entrained into the Karman street (red arrow) behind the mount support. Smoke streams flowing over the top of the thorax are attached back to a point behind the forewing hinge, but then separate as the top surface of the thorax descends towards the abdomen. Flow above the thorax is essentially linear and undisturbed. Flow behind the thorax is separated forming an unorganised bluff-body wake. In (C) the smoke intersects the wing at 1/4 wing length. The wings are stationary, but a Karman street behind the wings (red arrow), and slight downwards deflection of the smoke-streams indicates that they are held at some small positive static angle of attack. The flow below the insect is disturbed by the Karman street behind the mount support at the far downstream end of the image. In (D) the smoke intersects the wings at 3/4 wing length. As in (C) the flow over the wings themselves is attached, but a Karman street (red arrow) behind the trailing edge shows that the wings are held at some small positive static angle of attack. The flow is otherwise apparently laminar. (E) Here smoke hits the wing near the wingtip. The flow pattern remains similar to that seen further inboard in C and D, with a trailing Karman vortex street (red arrow).

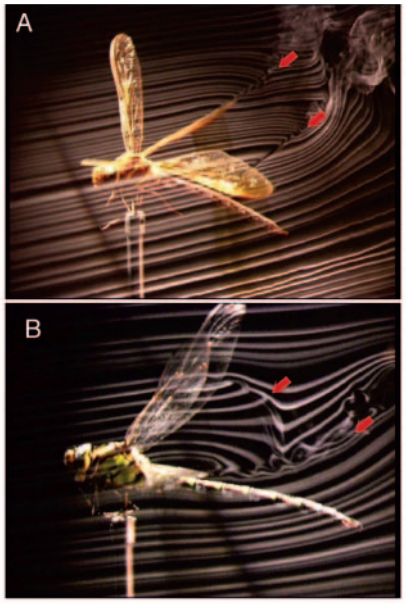

Fig. 11. Smoke visualization of tethered dragonflies flapping, but not generating any lift. (A) The dragonfly *Aeshna grandis* is flapping, but the aerodynamic angle of attack is sufficiently close to zero to generate no lift – as evidenced by the lack of any vertical displacement of the near-wake (red arrows). The wake shows that the wings have swept a straight path during the downstroke. In (B) (*Aeshna mixta*) the wake again shows that the wings can maintain an angle of attack at, or close to, zero, even when the forewing sweeps a curved path on the upstroke.

and compatible with the smokeline patterns we observed. The flow topology in counterstroking flight in dragonflies is not consistent with either the open negative bifurcation (Fig. 1A) or Werlé–Legendre (Fig. 1B) solutions for separated flows, because of the existence of a 3D free-slip critical point above the midline (Figs 12, 13). The topology of the dragonfly LEV is entirely consistent with the solution of the Navier–Stokes equations that yields a simple U-shaped separation (Fig. 1C).

Smokelines passing around the LEV become thinner (Fig. 14D) and bunch together (Figs 12A–I, 14A–E), indicating that flow is accelerated around the vortex. Smokelines accelerated around the vortex core develop undulations through Kelvin–Helmholtz instability (Saffman and Baker, 1979) in the shear layer at the boundary of the vortex core (Fig. 14E,D). This instability occurs where flows of differing velocity are separated by a distinct boundary layer: its occurrence above the wing conclusively demonstrates the presence of a shear layer (i.e. the separation surface). Instabilities just ahead of the separation line sometimes develop into secondary vortices, which may subsequently detach from the wing and travel around the vortex core (Fig. 14D).

Formation of a leading edge vortex through changes in angle of attack

The LEV typically forms during pronation, as the forewing rotates nose-down at the top of the stroke. Fig. 15 shows the sequence of LEV formation at midwing, and Fig. 16 shows the sequence of LEV formation and shedding above the thorax. Provided the relative timing of pronation and stroke reversal is appropriate to the rotational axis used (Dickinson et al., 1999; Sane and Dickinson, 2002), the angle of incidence of the freestream at the leading edge increases rapidly. The LEV grows maximally during the translation phase of the downstroke. The LEV remains attached throughout supination, as the forewing rotates nose-up at the bottom of the stroke: this rotation appears to occur around an axis near the leading edge of the wing, resulting in further dynamic increases in angle of attack which stabilises the LEV. Formation, growth and stabilisation of the LEV are therefore all associated with increases in angle of attack, resulting from either rotation or translation. Rapid increases in angle of attack can lead to LEV formation at any stage in the wingbeat – even on the hindwings (video S2 in supplementary material). Rapid decreases in angle of attack can likewise induce vortex shedding at any stage.

Shedding of the leading edge vortex

Occasionally, a LEV persisted on the dorsal surface of the forewings well into the upstroke, but usually the LEV was shed near the beginning of the upstroke and passed back over the hindwings (Fig. 16C,D), and the hindwing kinematics seem specifically configured to permit this mode of wake-capture, which has not previously been described for real insects (see also videos S1, S2 in supplementary material). In contrast to previous analyses of tethered hovering (Kliss et al., 1989), vortices are not built up over consecutive strokes of the same wing in forward flight: the wing kinematics seem configured to prevent interactions with wake elements shed on previous strokes, at least in forward flight.

Absence of starting vortices

A striking qualitative feature of LEV formation is the absence of a corresponding discrete starting vortex (Figs 12–16). Kelvin's theorem on persistence of circulation requires that the total circulation around any closed curve of particles in a fluid is constant, so any circulation generated by the wing must be balanced by opposite circulation in the wake. For impulsively started wings, the opposing circulation quickly rolls up into a starting vortex, inducing an unfavourable downwash at the wing. This diminishes lift, with full lift production only achieved after the wing has moved several chord lengths – a phenomenon called the Wagner effect (Wagner, 1925; Weihs and Katz, 1986). Real insect wings are not impulsively started, so aerodynamicists will not be surprised to find that a discrete starting vortex is not formed in dragonfly flight. Instead, the vortex sheet shed at the trailing edge rolls up into a series of small transverse vortices, rather than a single large starting vortex of comparable size to the LEV. These are clearly visualised in Fig. 14B–D. It is possible that the qualitative difference between the flows generated by free-flying dragonflies and those involved in the Wagner effect mean that the latter does not apply to dragonflies. Indeed, the

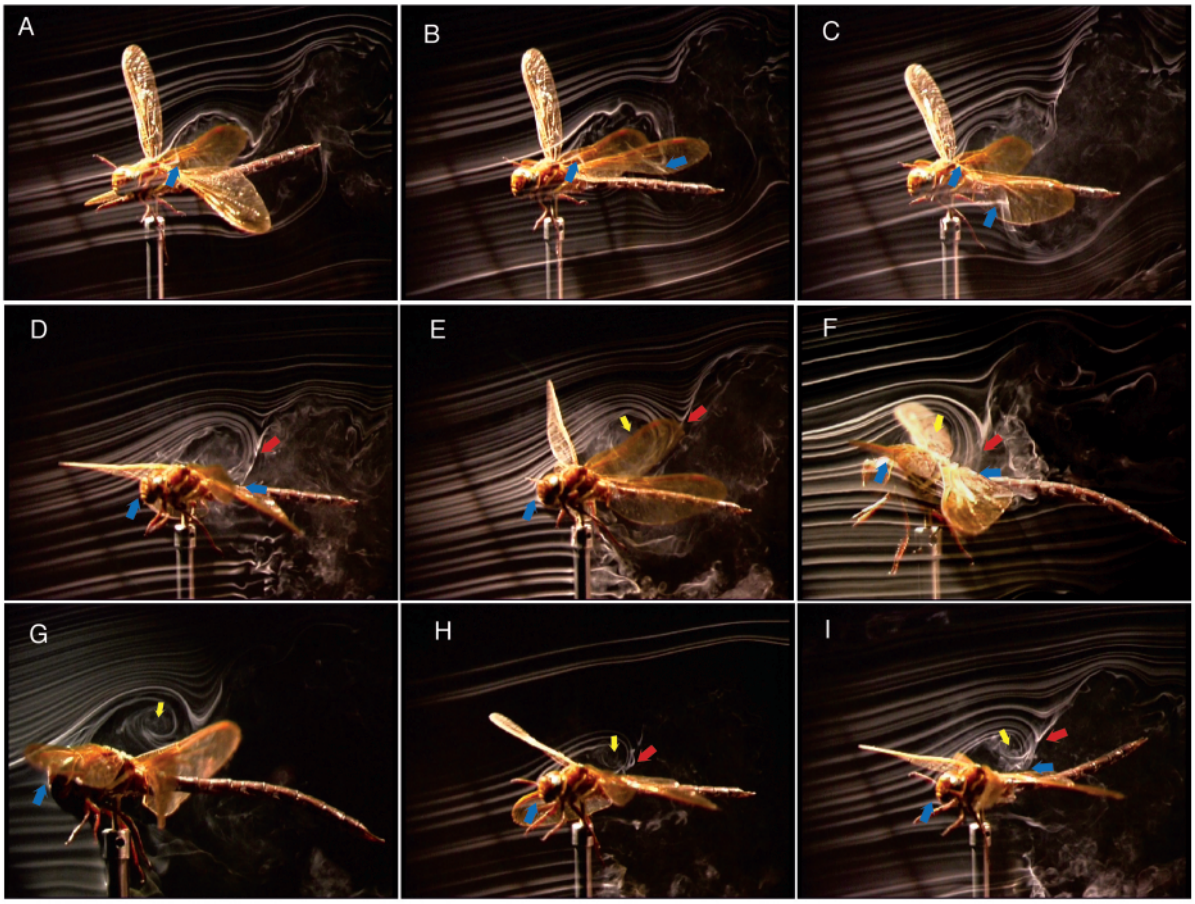

Fig. 12. Collection of flow visualization images selected to show the process of identification of critical points. Bifurcations in smoke streaklines are diagnostic of critical points. Blue arrows point to stagnation points either where a smoke stream hits the wings or head, or where the flow over the LEV touches down on the top surface of the wings, or on the body. Yellow arrows point to the free-slip critical point above the body. Red arrows point to smoke bifurcation at the saddle point in the wake caused by the shear layer between the downwash behind the attached LEV and the upwash of the LEV that was shed from the previous downstroke. (A–C) Flow over the wings at about half wing length. (D–F) Flow over the midline and interaction with the wake. (G–H) The free-slip critical point above the midline.

flow visualised in Fig. 14B–D is strikingly consistent with the classical lumped-vortex solution for the circulation and lift of an accelerated flat plate (see, for example, Katz and Plotkin, 2001, section 13.7), a solution which indicates that when the wake consists of a series of discrete vortices, rather than a single large starting vortex, there is only a slight loss of lift due to the downwash of the wake vortices (see, for example, Katz and Plotkin, 2001, fig. 13.8). Confirmation of this hypothesis would require quantitative data, but it is likely that the interactions between successive vortices in the shear layer behind the wings and viscous decay of the individual shear-layer vortices eliminates, or at least greatly reduces, the magnitude of the reduction in lift due to the Wagner effect. Qualitatively, the flow visualizations of Figs 14–16 make it unequivocally clear that at the start of the downstroke the dragonfly's wings operate in a flow field dominated by the upwash induced by the LEV shed from the previous downstroke (Fig. 15A). Irrespective of the Wagner effect, operating a wing in an upwash must increase the total lift-

Fig. 13. Smoke visualizations stepping across the thorax of *Aeshna grandis* in tethered flight. The flow pattern, shape, size and structure of the LEV is consistent at all positions across the thorax, and from wingbeat to wingbeat. (A–L) Oblique front views in which the dragonfly is traversed through the smoke plane in 1 mm steps from the far wing hinge across the thorax and out onto the near wing. There is a leading edge vortex in all images, and the shape and size of the LEV is consistent across the thorax and out onto the wing. (I-VI) Higher resolution side images. The dragonfly is traversed through the smoke plane in 2 mm steps so that the smoke impinges on the far side of the thorax in I, is on the midline and hits the dragonfly between the eyes in IV, and is out on the near wing base in VI. The blue arrows show the stagnation point where the separatrix touches down on the top of the thorax or hindwing. The shape and size of the leading edge vortex are strikingly consistent, even though the wing chord and velocity change dramatically as we step along the wing, across the narrow wing base onto the thorax. This is a remarkable result, suggesting that while the wings form the LEV the details of their shape, size and motion are not amongst the principle parameters controlling LEV morphology.

vector and should allow it to be tilted forwards at the start of the downstroke, which could lead to a substantial reduction in drag and increase in lift. Quantitative data are urgently required to measure the gain due to the beneficial interaction, at the start of the downstroke, between the wings and the wake shed from the previous downstroke.

Fig. 13.

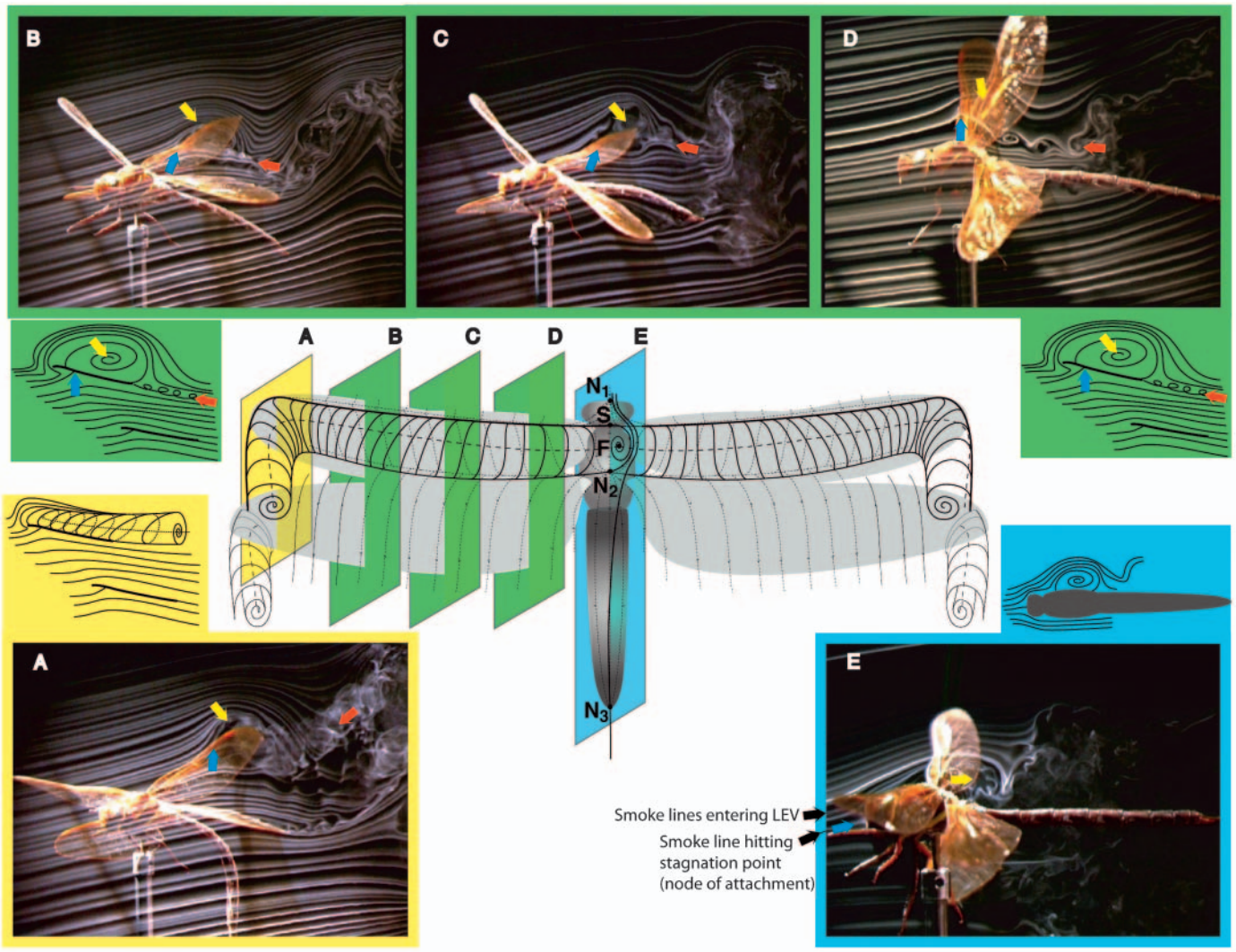

Fig. 14. Characteristic smoke patterns associated with the forewing downstroke in normal counterstroking flight. The video images show a tethered hawker *Aeshna grandis*; the topological interpretation is the same for all three species. The critical points in the 3D flow field are denoted by black spots (N=node; F=focus; S=saddle); dotted lines represent hypothetical surface streamlines. Visualizations are shown for 5 spanwise stations along the wing (A–E), marked by colour-coded slices in the figure. The LEV is continuous with the vortices trailing from the wingtips (A). The LEV diameter is similar across the wing, and the flow is topologically similar at all three stations inboard of the wingtip (B–D). The flow over the midline of the insect clearly shows that the LEV is continuous across the midline (E), indicating the existence of a free-slip focus above the thorax. The topology is the same throughout the downstroke: we have chosen those images that show the downstroke flow structures most clearly for each spanwise station.

Leading edge vortex formation with simplified kinematics – life-size flappers

We were able to replicate exactly both the gross flow topology and detailed qualitative features of the flow over dragonfly forewings with a mechanical model consisting merely of a flat plate in simple harmonic flapping, pitching or plunging motion (Fig. 17 and video S3 in supplementary material, which is an animation of Fig. 17; see also Taylor et al., 2003). Provided the flow velocity, frequency and amplitude combined to give a Strouhal number in the range $0.1 \leqslant St \leqslant 0.3$ (approximately the same as used by real dragonflies), detailed features of the flow topology over dragonfly forewings (Fig. 14) are accurately reproduced by the plunging or flapping plates (Fig. 17; see Taylor et al., 2003). A LEV forms as the angle of attack increases through translation at the start of the downstroke (Fig. 17B–D). Secondary vortices can be seen close to the separation line (Fig. 17C–H), and the smokelines can be seen spiralling into the vortex (Fig. 17C–F). As in real dragonflies, and in the parameter range $0.1 \leqslant St \leqslant 0.3$, there is no discrete starting vortex (Fig. 17B–F); instead the vortex sheet shed from the trailing edge rolls up under Kelvin–Helmholtz instability (Saffman and Baker, 1979) into a series of small transverse vortices of opposite sense to the LEV (Fig. 17C–G). Starting vortices could only be visualised outside of the range $0.1 \leqslant St \leqslant 0.3$. The LEV grows through most of the downstroke (Fig. 17B–F), rolling back from the

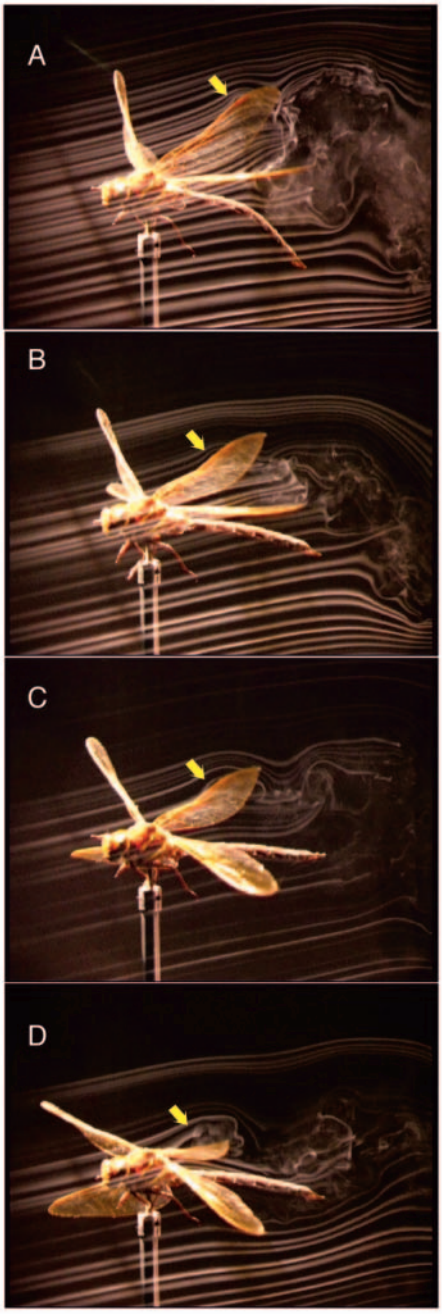

Fig. 15. LEV formation at the start of the downstroke in *Aeshna grandis* in counterstroking tethered flight. Yellow arrows point to the LEV throughout. In (A), a separation bubble can be seen on the top surface of the wing early in the phase of rotation (pronation) at the top of the upstroke prior to the beginning of the downstroke. The separation bubble begins at the leading edge, and flow reattaches at a point on the top surface between 1/4 and 1/2 of the way to the trailing edge. In (B) the wing has rotated further and begun to descend. The separation bubble is larger, with the separatrix reattaching on the top surface about 3/4 of the way from the leading edge to the trailing edge. In (C) the LEV has grown to cover the entire top surface of the wing, and shear is apparent behind the trailing edge between the forwards moving flow of the LEV and the backwards moving flow that has passed underneath the wing. The LEV is fully formed in (D).

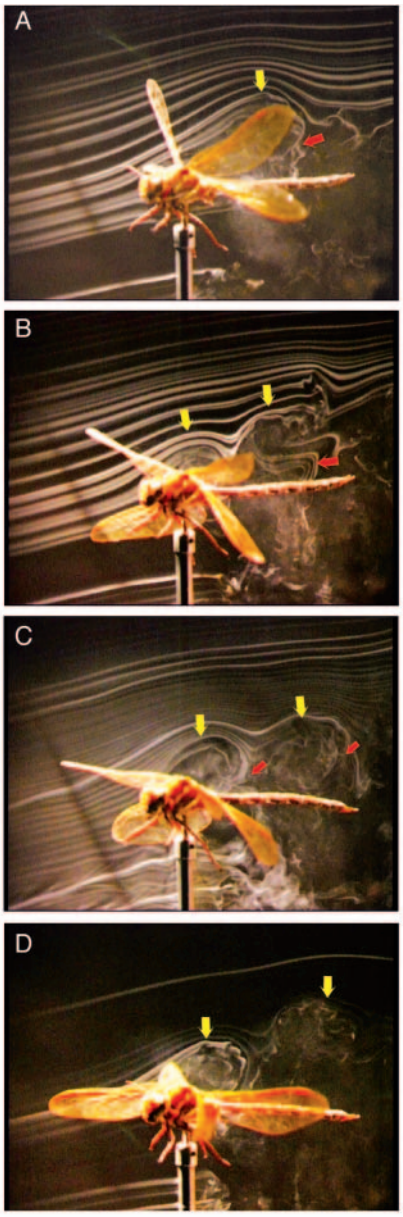

Fig. 16. LEV formation and growth in dragonflies. (A–D) Composite sequence of high-resolution centreline flow visualizations of tethered flight in *Aeshna grandis*. At the top of the forewing upstroke (A) the LEV shed after the previous downstroke is visible behind the wings in the wake (yellow arrow). There is a smoke bifurcation in the smoke streams behind the LEV (red arrow). In (B) at the start of the downstroke a LEV has formed between the forewings (left yellow arrow), and there is a second vortex in the wake (right yellow arrow), but this has the same sense of rotation as the LEV – as is clearly demonstrated by the pattern of smoke at the red arrow. Thus this second vortex is the shed LEV from the previous downstroke – representing a stopping vortex – and there is no evidence of the existence of any form of starting vortex. The wings clearly operate in a region influenced by the upwards flow to the left of the clockwise rotating shed vortex in the wake. By mid-downstroke (C), the LEV extends over the entire wing chord, and again there are only two coherent vortex structures visible (yellow arrows), and they have the same clockwise sense of rotation (as evidenced by the smoke at the red arrows). The LEV is transferred from forewing to hindwing at the end of the downstroke (D).

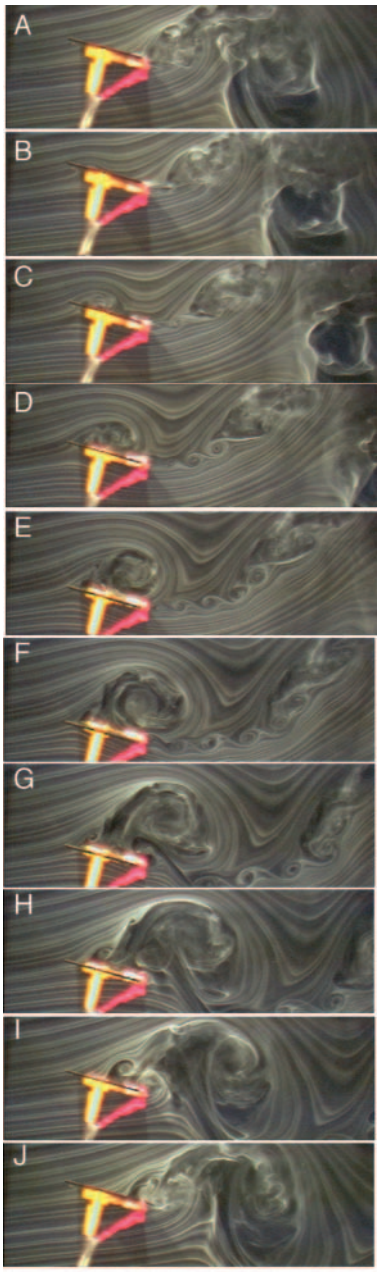

Fig. 17. LEV formation and growth on a flat plate plunging harmonically at 13 Hz in a 2.0 m s^{-1} flow (mean angle of attack 15°; 8 ms frame separation). Plunging is presented here because the plate never obscures the view – the flow field is similar in flapping or pitching motions (Taylor et al., 2003). (A–F) Detailed features of the flow topology over dragonfly forewings are reproduced with kinematics configured for $0.1 \leqslant St \leqslant 0.3$, as in real dragonflies. No starting vortex is produced: instead a vortex sheet forms in the shear layer behind the trailing edge (B–F), and transverse vortices of circulation opposite to the circulation of the LEV roll up under Kelvin–Helmholtz instability (C–G). The LEV grows through the downstroke (B–E) and translates back across the wing chord at the end of the downstroke (F). The LEV is eventually shed into the wake on the upstroke (G–J). Video S3 in supplementary material is an animation of this sequence including three additional intervening frames between every frame included in the figure.

leading edge towards the end of the downstroke (Fig. 17G). The LEV is shed earlier than in dragonflies. This is probably because the angle of attack decreases rapidly at the end of the downstroke: in dragonflies, the angle of attack is maintained or even increased as the wing rotates rapidly during supination at the end of the downstroke, which apparently stabilises the LEV. Complex wing kinematics are not *necessary* for LEV growth and formation.

The mechanical flapper demonstrates unequivocally that the LEV structure, including fine details such as the shear layer behind the trailing edge and secondary vortices, can be replicated even by a flat plate in flapping or plunging motion at the appropriate Strouhal number. This is critical because in a plunging motion there are no velocity gradients along the span to generate the pressure gradients required to produce a spanwise flow. In the absence of a spanwise flow there is no mechanism to transport chordwise vorticity along the axis of the LEV and out into the wingtip vortices. Nevertheless the LEV dwells on the wing for the duration of the downstroke provided the Strouhal number range is appropriate: the bottom of the downstroke is reached before the vortex grows so large as to be shed because of its size. This controlled qualitative experiment therefore demonstrates that spanwise flow is not *necessary* for the LEV to be stable throughout the downstroke, provided the Strouhal number is appropriate.

Discussion

In our dragonflies, and models, flapping kinematics are configured so that the Strouhal number is high enough that a LEV would be expected to form naturally over the wing and remain bound for the duration of the stroke. However, at any stage during the wingbeat, dragonflies can vary angle of attack from zero effective (aerodynamic) angle of attack up to a range that leads to immediate flow separation; whether a LEV actually forms, or is shed, is controlled by wing angle of attack. When a LEV is formed it extends continuously across the centreline of the dragonfly's thorax. The presence of this vortex on the line of symmetry allows us to rule out two of the three simplest known forms of flow separation (negative bifurcation lines and Werlé–Legendre separations) – the LEV structure is consistent with an open U-shaped separation. This is perhaps unsurprising, as this is the post-stall form of separation that occurs on a high aspect ratio wing (Katz and Plotkin, 2001). Other more complex forms of separation are known (Hornung and Perry, 1984; Perry and Chong, 1987), but as yet there is no evidence that they play any significant role in insect flight. Indeed, it makes sense for insects to avoid these more complex separations since they involve additional vortex elements that must require energy to form – causing drag, or requiring more muscle power output – but these extra vortex elements are not necessary for the formation of a LEV.

One of the most important conclusions of this study is the finding that in free-flying and tethered dragonflies, angle of attack controls aerodynamic mechanism through the wingbeat. Formation, growth and stabilisation of the LEV are all

associated with increases in angle of attack, whereas vortex shedding is associated with decreases in angle of attack. Changes in angle of attack can result from rotational and translational movements of the wings alike: it remains unclear whether rotational mechanisms differ qualitatively from other aerodynamic mechanisms involving changes in angle of attack (Walker, 2002). These conclusions are consistent with earlier work with mechanical flappers, which also found changes in angle of attack to play a key role in the dynamics of LEV formation, growth and shedding (Saharon and Luttges, 1987, 1988, 1989).

This same result may also explain some of the most important differences between our findings for free-flying dragonflies and the results of Luttges and colleagues. The first difference is that the flows they observed on tethered dragonflies (Kliss et al., 1989; Reavis and Luttges, 1988; Somps and Luttges, 1985) were always completely stalled. This is almost certainly an artefact of tethering, because we observed similar flow structures frequently in tethered flight, but only once in free flight (during a climb, where the flow over the forewing appears mildly stalled on a single downtroke; penultimate frame of video S2 in supplementary material). In steady flows, stall occurs when the angle of attack is above a certain critical value (roughly 15° for a high aspect ratio wing with a classical aerofoil such as the NACA0012). The same is true of unsteady flows, but rather higher angles of attack may be maintained – at least temporarily – if the flow separates from the leading edge and reattaches downstream such that the flow is not globally separated. Stalled flows may perhaps be important in hovering and during climbing manoeuvres, where extremely high local angles of attack may be unavoidable on some parts of the wings as a result of the flapping kinematics. However, our dragonflies' ability to maintain zero aerodynamic incidence during feathered strokes shows they can adjust aerodynamic angle of attack with a high degree of accuracy, and the fact that stalled flows do not normally appear in slow forward flight or even in turning manoeuvres is probably the deliberate result of controlling angle of attack. The fact that dragonflies maintain attached flows over the hindwings during normal counterstroking flight is further evidence that they usually control angle of attack so as to avoid stalled flows.

A second important difference between our results with free-flying dragonflies and those of Luttges and colleagues is that their mechanical flappers formed and shed multiple discrete vortex structures on each stroke (Saharon and Luttges, 1987, 1988, 1989). These vortices were found to interact in sequence to form a 'continuous multi-vortex structure', in which 'each vortex structure, however, remains a discrete entity' (Saharon and Luttges, 1989). This is quite different from any structure we found on either our tethered or free-flying dragonflies. Although secondary vortices were sometimes present in front of the LEV, these appear to result from flow instabilities at the separation line and from shear layer instabilities in the separation surface. We occasionally observed a small vortex to be shed immediately after pronation, but the normal pattern was for a single discrete LEV to form through each stroke. It is possible that the mechanical construction of Saharon and Luttges' flappers caused the formation of discrete vortex structures *via* backlash and step changes in angle of attack.

A third difference between our results and those of Luttges and colleagues cannot be explained by factors relating to adjustments in angle of attack. Saharon and Luttges describe the LEV generated by their mechanical flapper as forming '*a cone pattern*' with '*gradual reductions* [in vortex size] *associated with outboard span locations*', and state that '*the apex of this conical flow structure focuses on site [sic] where the apex of the wing tip vortex helix appears to originate*' (Saharon and Luttges, 1987). This is diametrically opposite to the form of the conical LEVs observed on other mechanical flappers and whirling arms (Birch and Dickinson, 2001; Dickinson et al., 1999; Usherwood and Ellington, 2002; Van den Berg and Ellington, 1997a,b), which apparently have a conical vortex originating from an apical focus near to the base of the wing. It is also completely different to the cylindrical form of the LEV observed in live dragonflies, which is continuous across the midline of the body and inflects near the wingtip to continue into the wingtip vortices with no apparent reduction in size (Fig. 4A). It is difficult to envisage why Saharon and Luttges (1987) would have found the LEV to decrease in size outboard along the span, when flapping velocity increases along the wing, and this may simply be an error in interpretation. In any case, our finding that the LEV is continuous across the midline in tethered and free-flying dragonflies cautions against drawing conclusions with respect to the flow topology from one-sided flappers, which cannot possibly generate this structure.

The result that the dynamics of LEV formation, growth and shedding in dragonflies can be accurately reproduced using a flat plate with simple kinematics configured to have a Strouhal number in the range $0.1 \leqslant St \leqslant 0.3$ is consistent with results from the mechanical flappers of Saharon and Luttges (1987, 1988, 1989). They found that the dynamics of LEV growth, formation and shedding depended strongly upon the reduced frequency parameter $k=fc\pi/U$. For a fixed wing morphology and stroke amplitude, the Strouhal number $St=fA/U$ differs from the reduced frequency by a constant factor. In the case of Saharon and Luttges' flapper, and assuming a stroke angle of 45°, St may be calculated from reduced frequency as $St \approx 0.5k$, so the reduced frequencies of $k=0.18$ and $k=0.5$ that they used correspond to approximately the same range of St as we used.

In fact, the Strouhal number is probably the fundamental aerodynamic parameter governing LEV dynamics (Anderson et al., 1998; Triantafyllou et al., 1993, 1991; Wang, 2000): the reduced frequency is also significant, but is unaffected by changes in stroke amplitude. Stroke amplitude is important because it is the product of stroke frequency and amplitude (which forms the numerator of the Strouhal number), rather than the product of stroke frequency and wing chord (which forms the numerator of the reduced frequency), that governs the speed of flapping. This in turn defines the maximum angle of attack that is attained through the stroke: for a given static

angle of attack, the maximum angle of attack during flapping increases with increasing Strouhal number. We have already said that angle of attack is the most important kinematic variable governing the aerodynamics of dragonfly flight, and this is consistent with the results from Saharon and Luttges' flappers (Saharon and Luttges, 1987, 1988, 1989). It is therefore natural that Strouhal number governs LEV dynamics, because it determines both the maximum angle of attack and the intrinsic timescales of flapping, which acts as a forcing function for the aerodynamics (Taylor et al., 2003).

It is nevertheless remarkable that even fine details of the flow topology on a dragonfly's wing can be replicated by the simple harmonic plunging of a flat plate at an appropriate Strouhal number. This suggests that a LEV may not be difficult for an animal with thin flapping wings to evolve. Fine-tuning of tandem wing interactions may be rather harder, and it is possible that the reason that counterstroking dragonflies use attached flows on the hindwings is to avoid complex interactions between vortices generated separately on the fore- and hindwing pairs. Parametric studies of the robustness of the hindwing–forewing interactions we have described – single LEV formation during in-phase stroking, and hindwing capture of the LEV shed by the forewings during counterstroking – must await future work with four-winged (i.e. two-sided) flappers. Saharon and Luttges (1989) also found that the hindwing of their tandem-winged flapper could trap vortex structures created by the forewing, but since the vortex structures then fused with those created by the hindwing, the details of the process are quite different (the hindwing generates no LEV in normal counterstroking flight in either tethered or free-flying dragonflies).

The smoke visualizations we have presented clearly distinguish between the hypotheses of Fig. 1. The LEV produced by dragonflies has the topology of a simple open U-shaped separation. The other hypotheses of Fig. 1 are rejected because there is a free-slip critical point over the midline, in free and tethered flight in dragonflies. The same topology has also been found in red-admiral butterflies (Srygley and Thomas, 2002). Dragonflies and butterflies bracket the entire range of wing morphology in insects – dragonflies have amongst the highest aspect ratios, butterflies amongst the lowest. The open U-shaped separation has the simplest possible vortex skeleton of any pattern of separation. It is also the natural separation that occurs in the unsteady post-stall flow over a high aspect ratio wing, or in dynamic stall. We therefore predict that formation of a LEV by means of an open U-shaped separation will be the typical high-lift aerodynamic mechanism involving flow separation in insects (and perhaps flying animals in general) with high aspect ratio wings.

One major implication of this result is that the root-flapping motion characteristic of all flying animals may be a constraint, imposed by the pre-existing musculo-skeletal structure, rather than an adaptation. A root-flapping motion is not *necessary* for any feature of the dragonfly LEV, and the dragonfly high-lift aerodynamic mechanism could be replicated (as we have shown) with a combination of appropriate pitching and plunging motions. This may be of some comfort to the micro-air-vehicle community.

This work was supported by BBSRC grants 43/S09380 and 43/S08664 to A.L.R.T. R.J.B. was supported by a BBSRC D.Phil studentship. A.L.R.T. was supported by a Royal Society University Research Fellowship for part of this work. G.K.T. is a Royal Society University Research Fellow, and was supported during this work by a Royal Commission for the Exhibition of 1851 Research Fellowship. a Weir Junior Research Fellowship at University College, Oxford and a Christopher Welch Scholarship.

References

Alexander, D. E. (1984). Unusual phase relationships between the forewings and hindwings in flying dragonflies. *J. Exp. Biol.* **109**, 379-383.

Alexander, D. E. (1986). Wind tunnel studies of turns by flying dragonflies. *J. Exp. Biol.* **122**, 81-98.

Anderson, J. M., Streitlien, K., Barrett, D. S. and Triantafyllou, M. S. (1998). Oscillating foils of high propulsive efficiency. *J. Fluid Mech.* **360**, 41-72.

Azuma, A., Azuma, S., Watanabe, I. and Furuta, T. (1985). Flight mechanics of a dragonfly. *J. Exp. Biol.* **116**, 79-107.

Azuma, A. and Watanabe, T. (1988). Flight performance of a dragonfly. *J. Exp. Biol.* **137**, 221-252.

Barlow, J. B., Rae, W. H. and Pope, A. (1999). *Low-speed Wind Tunnel Testing*, 3rd edn. New York: Wiley.

Birch, J. M. and Dickinson, M. H. (2001). Spanwise flow and the attachment of the leading-edge vortex on insect wings. *Nature* **412**, 729-733.

Birch, J. M., Dickson, W. B. and Dickinson, M. H. (2004). Force production and flow structure of the leading edge vortex on flapping wings at high and low Reynolds numbers. *J. Exp. Biol.* **207**, 1063-1072.

Bomphrey, R. J., Srygley, R. B., Taylor, G. K., Nudds, R. L. and Thomas, A. L. R. (2002). Visualising the flow around insect wings. *Phys. Fluids.* **14**, S4.

Bosch, H. (1978). Interfering airfoils in two-dimensional unsteady incompressible flow. *AGARD-CP-227*.

Chong, M. S., Perry, A. E. and Cantwell, B. J. (1990). A general classification of three-dimensional flow fields. *Phys. Fluids A* **2**, 765-777.

Délery, J. M. (2001). Robert Legendre and Henri Werlé: Toward the elucidation of three-dimensional separation. *Ann. Rev. Fluid Mech.* **33**, 129-154.

Dickinson, M. H., Lehmann, F.-O. and Sane, S. P. (1999). Wing rotation and the aerodynamic basis of insect flight. *Science* **284**, 1954-1960.

Ellington, C. P., van den Berg, C., Willmott, A. P. and Thomas, A. L. R. (1996). Leading-edge vortices in insect flight. *Nature* **384**, 626-630.

Hornung, H. and Perry, A. E. (1984). Some aspects of three-dimensional separation, Part I: Streamsurface bifurcations. *Z. Flugwiss. Weltraumforsch.* **8**, 77-87.

Huang, R. F., Wu, J. Y., Jeng, J. H. and Chen, R. C. (2001). Surface flow and vortex shedding of an impulsively started wing. *J. Fluid. Mech.* **441**, 265-292.

Jones, K. D. and Platzer, M. E. (1996). Time-domain analysis of low-speed airfoil flutter. *AIAA J.* **34**, 1027-1033.

Katz, J. and Plotkin, A. (2001). *Low-Speed Aerodynamics*. Cambridge: Cambridge University Press.

Kesel, A. B. (2000). Aerodynamic characteristics of dragonfly wing sections compared with technical aerofoils. *J. Exp. Biol.* **203**, 3125-3135.

Kida, S., Takaoka, M. and Hussain, F. (1991). Collision of 2 vortex rings. *J. Fluid Mech.* **230**, 583-646.

Kliss, M., Somps, C. and Luttges, M. W. (1989). Stable vortex structures: a flat plate model of dragonfly hovering. *J. Theor. Biol.* **136**, 209-228.

Lan, S. L. and Sun, M. (2001a). Aerodynamic force and flow structures of two airfoils in flapping motions. *Acta Mech. Sinica* **17**, 310-331.

Lan, S. L. and Sun, M. (2001b). Aerodynamic interactions of two airfoils in unsteady motion. *Acta Mech.* **150**, 39-51.

Lane, D. A. (1996). Visualizing time-varying phenomena in numerical simulations of unsteady flows. *AIAA*-1996-48.

Legendre, R. (1956). Séparation de l'écoulement laminaire tridimensionnel. *La Rech. Aérosp.* **54**, 3-8.

Lighthill, M. J. (1963). Attachment and separation in three-dimensional flow. In *Laminar Boundary Layers* (ed. L. Rosenhead), pp. 72-82. Oxford: Clarendon Press.

Lim, T. T. (2000). Dye and smoke visualization. In *Flow Visualisation: Techniques and Examples* (ed. A. J. Smits and T. T. Lim), pp. 43-72. London: Imperial College Press.

Maxworthy, T. (1979). Experiments on the Weis-Fogh mechanism of lift generation by insects in hovering flight. Part 1. Dynamics of the 'fling'. *J. Fluid Mech.* **93**, 47-63.

Maxworthy, T. (1981). The fluid-dynamics of insect flight. *Ann. Rev. Fluid Mech.* **13**, 329-350.

May, M. L. (1991). Dragonfly flight: power requirements at high speed and acceleration. *J. Exp. Biol.* **158**, 325-342.

Newman, B. G., Savage, S. B. and Schouella, D. (1977). Model tests on a wing section of an *Aeschna* dragonfly. *Scale Effects Animal Locomotion* **445**, 463-477.

Okamoto, M., Yasuda, K. and Azuma, A. (1996). Aerodynamic characteristics of the wings and body of a dragonfly. *J. Exp. Biol.* **199**, 281-294.

Olberg, R. M., Worthington, A. H. and Venator, K. R. (2000). Prey pursuit and interception in dragonflies. *J. Comp. Physiol. A* **186**, 155-162.

Peake, D. J. and Tobak, M. (1980). Three-dimensional interactions and vortical flows with emphasis on high speeds. *AGARDograph* **252**.

Perry, A. E. and Chong, M. S. (1987). A description of eddying motions and flow patterns using critical-point concepts. *Ann. Rev. Fluid Mech.* **19**, 125-155.

Perry, A. E. and Chong, M. S. (2000). Interpretation of flow visualization. In *Flow Visualisation: Techniques and Examples* (ed. A. J. Smits and T. T. Lim), pp. 1-26. London: Imperial College Press.

Perry, A. E. and Fairlie, B. (1974). Critical points in flow patterns. *Adv. Geophys. B* **18**, 299-315.

Perry, A. E. and Hornung, H. (1984). Some aspects of three-dimensional separation, Part II: Vortex skeletons. *Z. Flugwiss. Weltraumforsch.* **8**, 155-160.

Poincaré, H. (1882). Les points singuliers des équations différentielles. *C. R. Acad. Sci. Paris* **94**, 416-418.

Reavis, M. A. and Luttges, M. W. (1988). Aerodynamic forces produced by a dragonfly. *AIAA Paper 88-0330*.

Rüppell, G. (1989). Kinematic analysis of symmetrical flight manoeuvres of Odonata. *J. Exp. Biol.* **144**, 13-42.

Saffman, P. and Baker, G. (1979). Vortex interactions. *Ann. Rev. Fluid. Mech.* **11**, 95-122.

Saharon, D. and Luttges, M. W. (1987). Three-dimensional flow produced by a pitching-plunging model dragonfly wing. *AIAA Paper 87-0121*.

Saharon, D. and Luttges, M. W. (1988). Visualization of unsteady separated flow produced by mechanically driven dragonfly wing kinematics model. *AIAA Paper 88-0569*.

Saharon, D. and Luttges, M. W. (1989). Dragonfly unsteady aerodynamics: The role of wing phase relations in controlling the produced flows. *AIAA Paper 89-0832*.

Sane, S. P. and Dickinson, M. H. (2002). The aerodynamic effects of wing rotation and a revised quasi-steady model of flapping flight. *J. Exp. Biol.* **205**, 1087-1096.

Smits, A. J. and Lim, T. T. (ed.) (2000). *Flow Visualization. Techniques and Examples*. London: Imperial College Press.

Somps, C. and Luttges, M. (1985). Dragonfly flight – novel uses of unsteady separated flows. *Science* **228**, 1326-1329.

Somps, C. and Luttges, M. (1986). Dragonfly aerodynamics – response. *Science* **231**, 10-10.

Srygley, R. B. and Thomas, A. L. R. (2002). Unconventional lift-generating mechanisms in free-flying butterflies. *Nature* **420**, 660-664.

Su, W., Liu, M. and Liu, Z. (1990). Topological structures of separated flows about a series of sharp-edged delta wings at angles of attack up to 90°. In *Topological Fluid Mechanics: Proceedings of the IUTAM Symposium, Cambridge, August 13-18, 1989* (ed. H. K. Moffatt and A. Tsinober), pp. 395-407. Cambridge: Cambridge University Press.

Sunada, S., Zeng, L. and Kawachi, K. (1998). The relationship between dragonfly wing structure and torsional deformation. *J. Theor. Biol.* **193**, 39-45.

Taylor, G. K., Nudds, R. L. and Thomas, A. L. R. (2003). Flying and swimming animals cruise at a Strouhal number tuned for high power efficiency. *Nature* **425**, 707-711.

Tobak, M. and Peake, D. J. (1982). Topology of three-dimensional separated flows. *Ann. Rev. Fluid Mech.* **14**, 61-85.

Triantafyllou, G. S., Triantafyllou, M. S. and Grosenbaugh, M. A. (1993). Optimal thrust development in oscillating foils with application to fish propulsion. *J. Fluids Struct.* **7**, 205-224.

Triantafyllou, M. S., Triantafyllou, G. S. and Gopalkrishnan, R. (1991). Wake mechanics for thrust generation in oscillating foils. *Phys. Fluids A* **3**, 2835-2837.

Tuncer, I. H. and Platzer, M. F. (1996). Thrust generation due to airfoil flapping. *AIAA J.* **34**, 324-331.

Usherwood, J. R. and Ellington, C. P. (2002). The aerodynamics of revolving wings. I. Model hawkmoth wings. *J. Exp. Biol.* **205**, 1547-1564.

Van den Berg, C. and Ellington, C. P. (1997a). The three-dimensional leading-edge vortex of a 'hovering' model hawkmoth. *Phil. Trans. R. Soc. Lond. B* **352**, 329-340.

Van den Berg, C. and Ellington, C. P. (1997b). The vortex wake of a 'hovering' model hawkmoth. *Phil. Trans. R. Soc. Lond. B* **352**, 317-328.

Van Dyke, M. (1988). *An Album of Fluid Motion*. Parabolic Press, Stanford, CA.

Wagner, H. (1925). Über die Entstehung des dynamischen Auftriebes von Tragflügeln. *Z. Angewandte Math. Mech.* **5**, 17-35.

Wakeling, J. M. and Ellington, C. P. (1997a). Dragonfly flight. I. Gliding flight and steady-state aerodynamic forces. *J. Exp. Biol.* **200**, 543-556.

Wakeling, J. M. and Ellington, C. P. (1997b). Dragonfly flight. II. Velocities, accelerations and kinematics of flapping flight. *J. Exp. Biol.* **200**, 557-582.

Wakeling, J. M. and Ellington, C. P. (1997c). Dragonfly flight. III. Lift and power requirements. *J. Exp. Biol.* **200**, 583-600.

Walker, J. A. (2002). Rotational lift: something different or more of the same? *J. Exp. Biol.* **205**, 3783-3792.

Wang, Z. J. (2000). Vortex shedding and frequency selection in flapping flight. *J. Fluid Mech.* **410**, 323-341.

Wang, Z. J., Birch, J. M. and Dickinson, M. H. (2004). Unsteady forces and flows in low Reynolds number hovering flight: two-dimensional computations vs robotic wing experiments. *J. Exp. Biol.* **207**, 449-460.

Weihs, D. and Katz, J. (1986). Transient induced drag. *AIAA J.* **24**, 1203-1205.

Werlé, H. (1962). Separation on axisymmetric bodies at low speed. *Rech. Aéro.* **90**, 3-14.

Werlé, H. (1974). Le Tunnel Hydrodynamique au Service de la Recherche Aerospatiale, Publ. no. 156, ONERA, France.

Willmott, A. P., Ellington, C. P. and Thomas, A. L. R. (1997). Flow visualization and unsteady aerodynamics in the flight of the hawkmoth, *Manduca sexta*. *Phil. Trans. R. Soc. Lond. B* **352**, 303-316.

Wood, E. R., Powers, R. W., Cline, J. H. and Hammond, C. E. (1985). On developing and flight testing a higher harmonic control system. *J. Am. Heli. Soc.* **30**, 1.

Wootton, R. J., Kukalová-Peck, J., Newman, D. J. S. and Muzón, J. (1998). Smart engineering in the mid-Carboniferous: how well could Palaeozoic dragonflies fly? *Science* **282**, 749-751.

Yates, G. T. (1986). Dragonfly aerodynamics. *Science* **231**, 10-10.